Behavior of Circular Fiber-Reinforced Polymer–Steel-Confined Concrete Columns Subjected to Reversed Cyclic Loads: Experimental Studies and Finite-Element Analysis

Yanlei Wang[1]; Gaochuang Cai[2]; Yunyu Li[3]; Danièle Waldmann[4]; Amir Si Larbi[5]; and Konstantinos Daniel Tsavdaridis[6]

Abstract: This paper studied experimentally the behavior of circular fiber-reinforced polymer (FRP)–steel-confined concrete columns subjected to reversed cyclic loads. The influence of main structural factors on the cyclic behavior of the columns is discussed. Test results showed the outstanding seismic performance of FRP–steel-confined RC and steel-reinforced concrete (SRC) columns. The lateral confinement effectiveness of glass fiber–reinforced polymer (GFRP) tubes and GFRP–steel tubes was verified and a simplified OpenSees-based finite-element method (FEM) model was developed to simulate the experimental results of the test columns. Based on the proposed FEM model, a parametric analysis was conducted to investigate the effects of main factors on the reversed cyclic behavior of GFRP–steel-confined RC columns. Based on the test and numerical analyses, the study discussed the influence of variables such as the lateral confinement on the plastic hinge region (PHR) height and peak drift ratio of the columns under reversed cyclic loads. Results indicate that lateral confinement significantly affects the PHR height of circular confined RC columns. Based on the analyses of the data from this study and literature, a simple model was suggested to predict the peak drift ratio of confined RC columns. **DOI: 10.1061/(ASCE)ST.1943-541X.0002373.**

Author keywords: Seismic behavior; Fiber-reinforced polymer (FRP); Lateral confinement; Plastic hinge region; Composite structure; Hysteresis behavior.

Introduction

It is generally accepted that properly confined concrete can develop adequate ductility for RC elements, allowing sufficient lateral deformability without a significant reduction in strength. For RC beams and columns, confinement is usually located at the plastic hinge regions (PHRs) by using different external constraints such as steel tubes (Tomii 1985a, b) and fiber-reinforced polymer (FRP) sheets (Teng et al. 2002). Moreover, the confinement can further enhance the deformability and ductility of RC columns subjected to reversed cyclic loads, which is meaningful for concrete structures in seismic regions or for high-rise buildings. This is because unconfined concrete elements might fail due to damage accumulation during reversed cyclic loads, thus leading to further damage or the collapse of whole structure.

Fig. 1 shows the main confinement methods of two kinds of concrete elements: (1) RC, and (2) concrete-filled steel tube (CFST) elements. For the former, the addition of external steel tube confinement was suggested to improve the ductility, deformation, and damage control of the concrete cover of RC elements. The concept of tubed columns was first introduced to the research community by Tomii et al. (1985a, b), and is called steel tube–confined columns. The lateral tube confinement significantly enhances the bearing capacity of the RC elements. Additionally, the external steel tube can work as a part of the formwork system to accelerate construction. Steel tube–confined concrete (STCC) elements initially were used in the construction industry and presented excellent deformation ability and ductility, which was attracted by research community worldwide. This can be attributed to the fact that the STCC effectively avoids outward local buckling (OLB) for the local yielding of the steel tube under large loads or at large lateral deformation (Tomii et al. 1985a, b; Sakino et al. 2004), which usually occurs in CFST elements. Additionally, the steel tube is designed not to carry directly axial loads in STCC elements via the termination of the steel tube at its two ends. Furthermore, STCCs provide a solution to overcome the difficulty of the load transfer mechanisms and the detailing design at RC beam-to-CFST

[1]Associate Professor, State Key Laboratory of Coastal and Offshore Engineering, School of Civil Engineering, Dalian Univ. of Technology, Dalian 116024, China. ORCID: https://orcid.org/0000-0001-9022-3918

[2]Assistant Professor, Dept. of Architecture, Faculty of Engineering, Fukuoka Univ., Fukuoka 814-0180, Japan; Invited Professor, Laboratoire de Tribologie et de Dynamique des Systèmes, Ecole Nationale d'Ingénieurs de Saint-Etienne, Univ. Lyon, UMR 5513, 58 Rue Jean Parot, 42023 Saint-Etienne Cedex 2, France (corresponding author). ORCID: https://orcid.org/0000-0003-2847-0699. Email: gaochuang.cai@enise.fr; cai@fukuoka-u.ac.jp

[3]Lecturer, School of Transportation, Wuhan Univ. of Technology, Wuhan 430063, China. Email: liyunyu@whut.edu.cn

[4]Associate Professor, Laboratory of Solid Structures, Univ. of Luxembourg, Maison du Nombre, 6, Ave. de la Fonte, Esch-sur-Alzette L-4364, Luxembourg. ORCID: https://orcid.org/0000-0002-8345-0474

[5]Full Professor, Laboratoire de Tribologie et de Dynamique des Systèmes, Ecole Nationale d'Ingénieurs de Saint-Etienne, Univ. Lyon, UMR 5513, 58 Rue Jean Parot, 42023 Saint-Etienne Cedex 2 France.

[6]Associate Professor, School of Civil Engineering, Univ. of Leeds, Woodhouse Lane, Leeds LS2 9JT, UK.

Note. This manuscript was submitted on April 23, 2018; approved on January 10, 2019; published online on June 25, 2019. Discussion period open until November 25, 2019; separate discussions must be submitted for individual papers. This paper is part of the ***Journal of Structural Engineering***, © ASCE, ISSN 0733-9445.

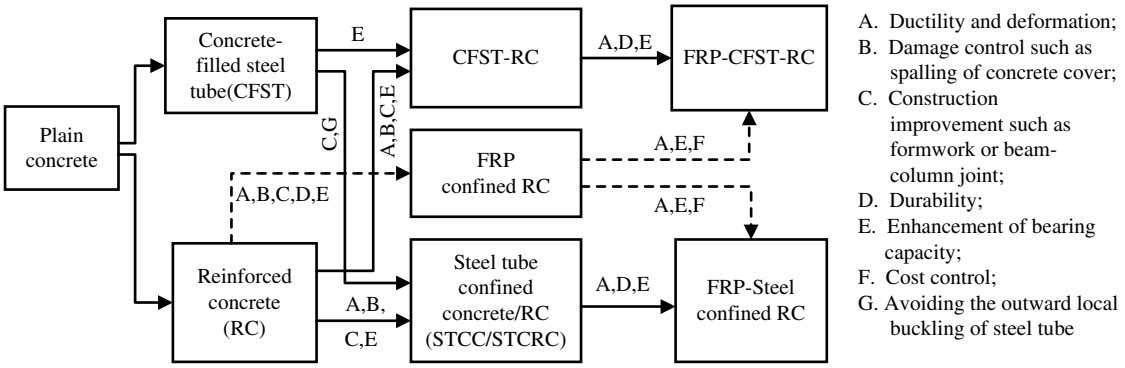

Fig. 1. Development of RC and confined concrete in past decades.

column joints. A number of studies have been conducted to understand the constitutive behavior (Binici 2005; Li et al. 2005) and structural behavior of STCCs under various loads (Aboutaha and Machado 1999). In particular, Han et al. (2005) experimentally investigated the monotonic and cyclic behaviors of STCC columns, Han et al. (2009) experimentally investigated thin-walled STCC column-to-beam joints, and Han et al. (2008) experimentally investigated thin-walled STCC columns subjected to axial local compression. Zhou and Liu (2010) experimentally studied the seismic behavior and shear strength of STCC short columns, Zhou et al. (2015, 2016) experimentally studied the performance of STCC columns under eccentric compression, and Zhou et al. (2017) experimentally studied the behavior of circle STCC column-to-RC beam connections under axial compression. In addition, Yu et al. (2010) proposed a finite-element method (FEM) analysis model to analyze the mechanisms of STCC columns under axial compression.

However, the buckling of the steel tube in CFSTs at large deformation and its corrosion in aggressive environments limits their application in civil engineering; similarly, corrosion of the steel tube also obstructs the application of STCCs in an aggressive environment. According to the literature (Wu et al. 2014; Liu et al. 2018), the FRP wrapping of the STCC solves the durability concerns of STCC structures. However, a few concerns regarding this kind of structural elements still need to be addressed, such as low longitudinal stiffness and relatively high construction cost. Therefore, a FRP–steel-confined RC element has been developed. Ran (2014) and Huang (2016) investigated the constitutive behavior of GFRP-STCC under monotonic and cyclic axial loads. Cao et al. (2017) experimentally investigated the behavior of FRP-STCC stub columns with expansive self-consolidating concrete under axial compression. Liu et al. (2018) studied the axial behavior of circular CFRP-STCC stub columns. In summary, compared with STCC and FRP-confined concrete structures, FRP-STCC structures are more durable and flexible because of the durable FRP materials and a more effective confinement.

On the other hand, CFST elements are popular in high-rise buildings or piers in Europe and Japan, where RC is widely applied. This is due to the reasonable arrangement of steel and concrete in the section, which optimizes the sectional strength and stiffness of the elements, leading to an effective use of the material properties to resist tension and bending actions in the section. In addition, the tube can serve as a part of formwork in construction, which decreases labor and material costs. However, the effects of the bond, confinement, and OLB on CFST structural behavior are under study to facilitate the development of design methods of members under lateral reversed cyclic loads. External FRP confining may be a potential solution to fix the OLB problem of CFST elements (Xiao 2004; Hu et al. 2011) because of the high-strength and elastic properties of FRP materials, but this is still under study. Xiao (2004) proposed FRP-confined CFST columns, and compared FRP-STCC and CFST elements. Xiao concluded that a FRP-confined CFST column combines the advantages of a conventional CFST column and a tubed column, in which additional transverse reinforcement is designed for the potential plastic hinge regions to improve the seismic performance of the elements. Xiao et al. (2005) performed a study to introduce and experimentally validate FRP-confined CFST columns under axial and seismic loads, and confirmed the excellent seismic performance of these columns. Recently, several studies examined the constitutive behavior of FRP-confined CFST columns (Xiao et al. 2005; Liu and Lu 2010; Park et al. 2010; Tao et al. 2011; Lin 2012; Teng et al. 2013; Park and Choi 2013; Hu and Seracino 2014; Wang et al. 2015; Yu et al. 2016), but more studies are underway to examine details of the elements.

Only limited studies of the structural behavior of FRP-STCC elements under various loads are currently available in the literature. Most of the studies focused on the behavior of the elements under axial compressive loads (Cao et al. 2017; Liu et al. 2018). Therefore, the major objective of this paper was to study the behavior of circular GFRP-STCC columns under combined constant axial loads and lateral reversed cyclic loads. Based on experimental observations and analyses of the deformation mechanisms, this paper also proposes a FEM analysis model to simulate the structural response under the combined loads. Moreover, this study discussed the effect of the main structural design factors on the behavior of FRP-STCC columns under reversed cyclic loads.

Experimental Program

Test Overview

In this experiment, eight circular-sectional concrete columns were designed and prepared, including one RC column, one steel tube–confined RC column, one steel tube–confined steel-reinforced concrete (SRC) column, one CFRP–steel-confined RC column, two GFRP–steel-confined RC columns, and two GFRP–steel-confined SRC columns. The core concrete diameter of all specimens was 300 mm and the thickness of the concrete cover was 30 mm. The height of the columns was 1,350 mm with a 300-mm-high column head. The dimension details and steel arrangement of the specimens are presented in Fig. 2. The volumetric ratio of longitudinal

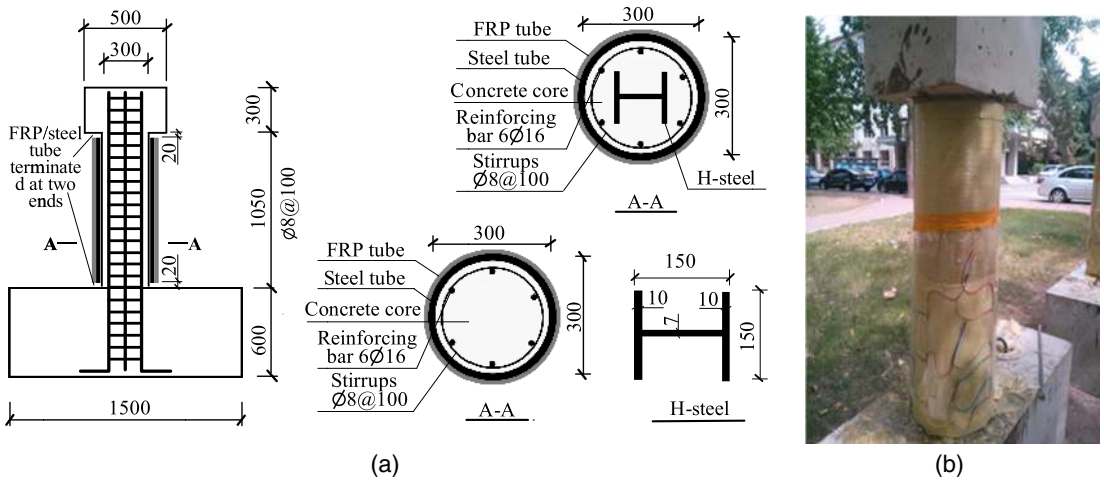

Fig. 2. Details of test specimens (units: millimeters): (a) dimension and reinforcement arrangement; and (b) confined columns.

Table 1. Details of test specimens

Test No.	Diameter, D (mm)	Thickness, t_s (mm)	Reinforcing bars	Stirrups	Number of layers of FRP sheet	FRP type	Setting of H-steel
G0S0T0	300	—	6Φ16	Φ8@100	—	—	No
G0S1T0	300	3			—	—	No
G5S1T0	300	3			5	GFRP	No
G7S1T0	300	3			7	GFRP	No
C7S1T0	300	3			7	CFRP	No
G0S1T1	300	3			—	—	Yes
G5S1T1	300	3			5	GFRP	Yes
G7S1T1	300	3			7	GFRP	Yes

Note: Gx/Cx = x layers GFRP/CFRP sheet; S0/S1 = without/with confined steel tube; and T0/T1 = without/with H-steel.

steel bar of all specimens was 1.71%, and the stirrup volumetric ratio was 0.6%. For the steel tube–confined specimens, the thickness of the steel tubes was 3.0 mm. In order to prevent the direct axial compression of the steel tubes, 20-mm gaps were set at both ends of the columns. In FRP-confined specimens, FRP was used to confine the hinge zone of 500 mm with different layers depending on the test design, whereas the remaining parts of the columns were wrapped in two layers of the same type of FRP sheet. For the confined SRC columns, standard H-section steel ($150 \times 150 \times 10 \times 7$ mm) was set from underneath the base beam to the top of the column. Table 1 and Fig. 2(a) give the details of the test specimens.

Specimen Manufacture

All steel tubes in the study were manufactured from 3.0-mm steel plates by welding at their lap zone. The tested specimens were prepared in following the steps: (1) setting of the reinforcement cage of columns and base beam; (2) setting of the steel tube (its welding line was placed on the plane oriented parallel to the column's axis of symmetry); (3) setting of the reinforcement cage and module of the stigma (column head); (4) curing of the specimens; and (5) removing the steel tube for concrete columns or wrapping FRP sheet for FRP–steel-confined concrete columns. The key steps of FRP wrapping were as follows: (1) polishing the surface with an angle grinder to enhance its surface roughness; (2) cleaning the surface of the steel tubes, such as by wiping them with alcohol; and (3) setting of FRP sheet. The overlap length of FRP wrapping was about 300 mm and the welding line of the steel tube was located in the middle of the overlap zone of FRP wrapping to prevent cracking of the welding line. Fig. 2(b) shows a completely GFRP–steel-confined column specimen.

Material Properties

Two kinds of unidirectional FRP sheets were used, i.e., GFRP sheet L900 (900 g/m^2) and CFRP sheet UT70-30 (300 g/m^2). A construction impregnation adhesive for structural application, an epoxy adhesive, was used, the properties of which are listed in Table 2. Ready-mixed concretes were used which contained 5–10-mm aggregates with a target compressive strength of 40 MPa. According to the test results of six standard concrete cubes ($150 \times 150 \times 150$ mm), the cube compressive strength of concrete was 41.2 MPa, which wasapproximate used as the approximate concrete cylinder compressive strength by multiplying it by 0.8 for normal-strength concrete. The transverse and longitudinal reinforcements of the columns were 8-mm plain (smooth) steel rebars and 16-mm deformed steel rebars, respectively. Q235 steel tube (3.0-mm thickness) was used to confine the columns, the properties of which are listed in Table 2 as obtained by the standard test method, GB/T228-2010 (Chinese Standards 2009). Standard H-section steel ($150 \times 150 \times 10 \times 7$ mm) was used in the tested SRC columns (Fig. 2).

Test Setup and Measurement

The details of the test setup are illustrated in Fig. 3. The bottom base beam of each specimen was first anchored on a strong RC floor with several high-strength steel bolts. At the ends of the beam,

Table 2. Material properties of steel, FRP, and epoxy adhesive

Material	Diameter or thickness (mm)	Young's modulus, E_s (GPa)	Yielding strength, f_y (MPa)	Tensile strength, f_u (MPa)	Elongation, δ (%)
Steel tube, Q235	3	210	280	414	—
Stirrups, Q345	8	206	400	540	—
Reinforcing rebar, Q345	16	205	420	590	—
H-steel wing/web plates	10/7	208/221	223/225	374/387	—
CFRP	0.167	245	—	4,077	1.51
GFRP	0.354	72	—	1,500	2.1
Epoxy	—	≥2.4	—	≥38	≥1.50

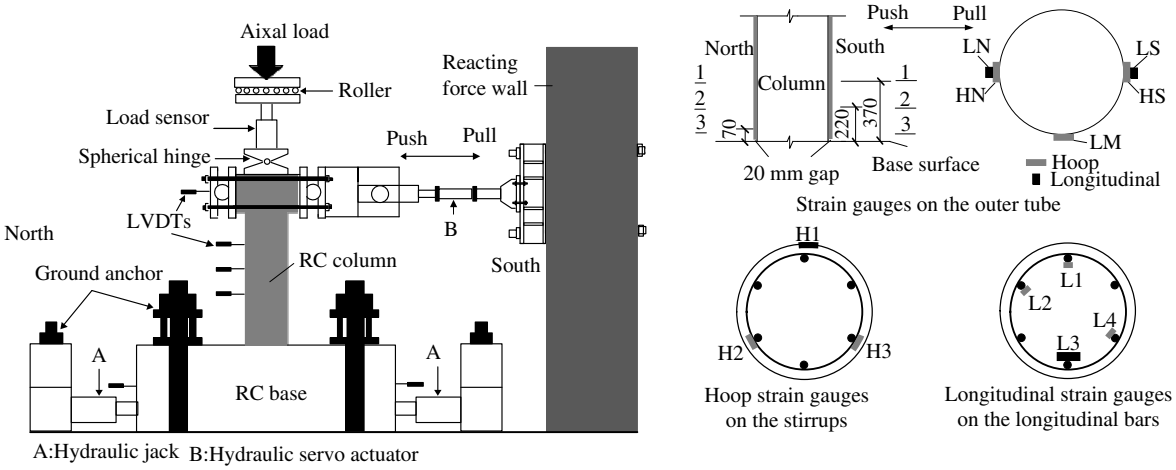

Fig. 3. Test setup and layout of LVDTs and strain gauge (units: millimeters).

two LVDTs were used to record its possible slipping during the test. Constant axial loads were applied on the top of the columns by a hydraulic jack with a maximum capacity of 1,000 kN (Fig. 3). The reversed lateral cyclic load was applied at the column head using a hydraulic jack with a maximum capacity of 1,000 kN with a one-way steel hinge device that could rotate around the vertical and horizontal loading directions. The applied axial load in each column was designed as 978 kN for RC columns and 1,242 kN for SRC columns—about 35% of the nominal axial load capacity (N) of the columns obtained as per the Chinese standards GB 50010-2010 (Chinese Standards 2015) and JGJ3-2002 (Chinese Standards 2002).

During the tests, the lateral load and displacement of the columns were monitored using one load cell and several LVDTs (450, 600, and 750 mm from the top of the base beam), whereas the strains of the longitudinal reinforcement, stirrup, FRP-steel tube, and steel tube during the loading were investigated using several gauges. Four strain gauges (L1–L4) and three hoop strain gauges (H1–H3) were installed on the longitudinal rebars and on the stirrups, respectively, at a distance of about 10 mm from the top of the base beam. Two hoop strain gauges (HN and HS) and three vertical strain gauges (LN, LS, and LM) were arranged on the surface of the steel tube or the FRP tube, respectively, at distances of 70, 220, and 370 mm from the top of the base beam, in order to measure the horizontal and vertical strains of the steel tube or the FRP tube.

Loading Methods

It was necessary to establish a reasonable loading history to capture the critical issues of the resistance and deformation of structural elements during the quasi-static cyclic loading tests. After the application of a constant axial load on top of the columns, a multiple reversed cyclic lateral loading was performed on each column. In the reference column, a deformation-controlled reversed cyclic lateral loading was applied with an increment of 4.0 mm. The target deformation of the first cyclic loading was 4.0 mm. When the lateral displacement reached 12 mm, the lateral loading was repeated twice at each target cycle of lateral loading. A similar loading method was performed on the confined concrete columns, except that the increment of lateral deformation was set as 8.0 mm after the lateral displacement of the columns exceeded 16 mm. For security, the tests were ended if the lateral resistance force of the specimen decreased to 60% of its maximum measured value or if the lateral displacement of the columns was too large, such as over 100 mm. Fig. 4 presents the loading procedure applied on the columns.

Test Observations

Cracking Evolution and Damages

RC Column and Steel Tube–Confined RC Column (G0S0T0 and G0S1T0)

In Specimen G0S0T0, the first horizontal crack occurred at the north side of the column about 100 mm from the top of the base beam. Then a semicircular horizontal crack appeared on the south side at a height of 100 mm. At the same time, a second crack appeared at a north side of the column, at a height of 200 mm. Meanwhile, horizontal cracks began to appear in the upper part and in the middle of the south side and began to develop to the north side of the column. Next, new horizontal cracks appeared in the columns about 400 and 600 mm from the top of the base beam. With the

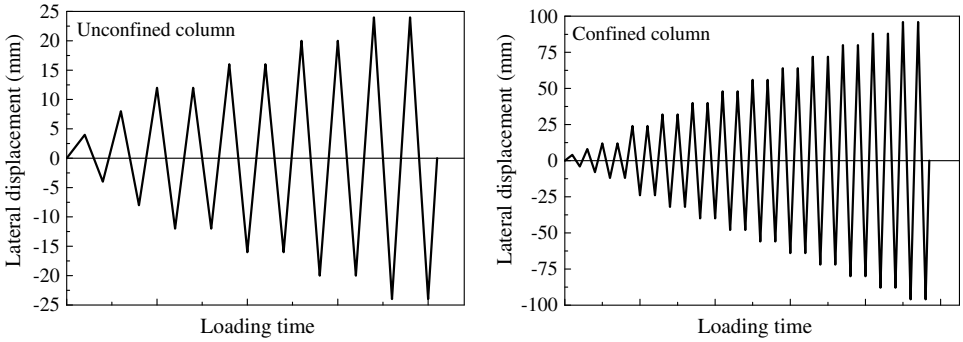

Fig. 4. Loading procedure.

increase of the lateral displacements, the cracks below the south side developed and the horizontal cracks continued to develop, and crushing of the concrete at the south side of columns occurred. At this time, the first vertical crack was confirmed in the south-side concrete, along with crushing of the concrete on the north side. Next, at the north side of the concrete, the first vertical cracks appeared. When the lateral displacement was about 24 mm, the concrete cover on the north side had a large area of spalling, but a buckling of the longitudinal reinforcing bar could not be observed. All the damages and cracks in the column were mainly caused by the plastic deformation of concrete and internal damage surrounding the deformed reinforcements. The final failure morphology of the specimen is shown in Fig. 5.

In the steel tube–confined RC column, G0S1T0, the early stage cracks could not be visually observed due to the external steel tube. When the lateral displacement was 48 mm, cracking and extrusion exfoliation of concrete were found at the bottom of the column. After removing the steel tube at the end of the column, the concrete at the bottom of the confined zone was crushed, but due to the constraints of the steel tube, it did not fall off. Several slipped shear cracks were also found at the foot of the column. All damages and cracks were still caused by the plastic deformation of the elements; however, the confinement of the steel tube effectively reduced the crushing of the concrete, which indicates that the failure of the column differs from that of RC columns, in which sectional concrete crushing is one of main reasons of structural failure.

FRP–Steel-Confined RC Columns (G5S1T0, G7S1T0, and C7S1T0)

Specimen G5S1T0 had a large residual displacement after testing. At the surface of the GFRP tube wrapped in the column foot, the resin slightly cracked. After removing the GFRP wrapping and steel tube, several cracks were found at the column foot and the south side of the column. This was because the compression from the upper part of the north side GFRP–steel-confined concrete promoted the crushing to the concrete below (about 50 mm from the top of the base beam). However, damage of the outermost layer of GFRP tube did not appear during testing. Compared with Specimen G5S1T0, two more layers of GFRP sheets were applied to Specimen G7S1T0, but the failure mode of the two specimens was similar. When the lateral displacement was too large, the concrete at the top of the base beam disintegrated. Upon removing the GFRP tube and steel tube after testing, several horizontal and diagonal cracks were observed at a distance of 100 mm from the top of the base beam. However, the confinement of the GFRP was able to protect the core concrete in a satisfactory manner. Compared with Specimen G7S1T0, when GFRP was replaced with CFRP, a similar failure mode, cracking pattern, and damage were found in Specimen C7S1T0, so it can be stated that the confinement of the columns was performant. In summary, the main damages and cracks of FRP–steel-confined RC columns concentrated on the critical section between the column and the base beam, and manifested as crushing and slipped cracks, respectively.

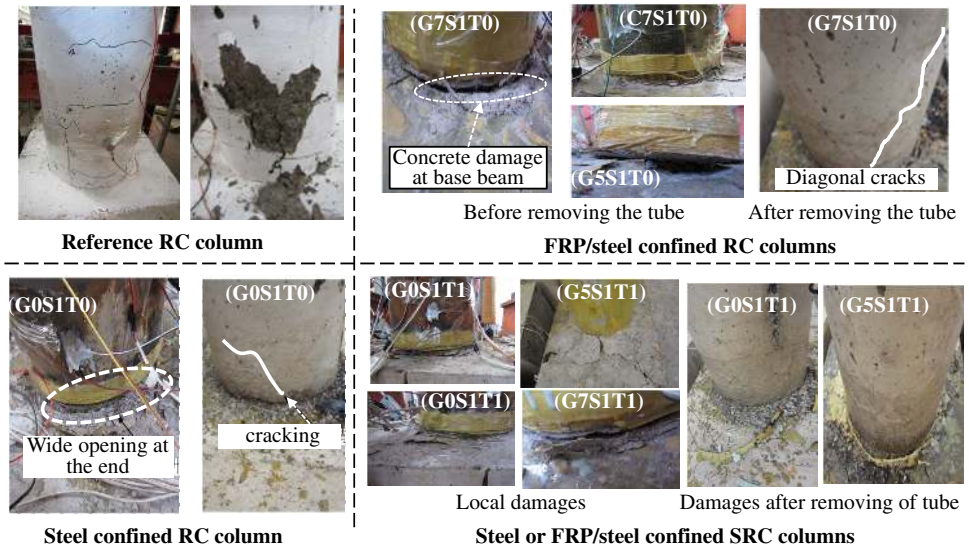

Fig. 5. Damages and cracks of the specimens.

FRP–Steel-Confined SRC Columns (G0S1T1, G5S1T1, and G7S1T1)

The cracks and damages of the steel tube–confined SRC column G0S1T1 were similar to that of the steel tube–confined RC column G0S1T0. When the lateral displacement increased to about 48 mm, the parts of the concrete on the top of the base beam and the column foot were cracked and damaged as the steel tube deformed and stretched continuously. At the end of the test, there was no apparent buckling or other failure characteristics visible on the steel tube. When removing the steel tube later, a horizontal crack was observed at about 80 mm near the column foot, but there was no other damage to the column body. When the steel tube was confined by GFRP tube, such as in Specimen G5S1T1, the cracks appeared on the south side of the column above the base beam when the lateral displacement of the column was 25 mm. These cracks developed further into compressive damage of the concrete cover. At the end of the experiment, however, the confined concrete was still almost intact. Compared with the case of Specimen G5S1T1, the cracks and damages were controlled well when using more layers of GFRP sheets in G7S1T1. However, the failure mode of this specimen was similar to that of Specimen G5S1T1. In the case of large displacement, the concrete at the top of the base beam initially disintegrated, before being damaged near the top of the column. Finally, the concrete was damaged at around 10 mm over the base beam, whereas the confined concrete remained protected, without visual horizontal or diagonal cracks. In summary, the damages and cracks in the confined SRC columns were much smaller than those of the other columns, which was attributed to the reinforcement of the strong H-section steel inside.

Hysteresis Behavior

RC and Steel Tube–Confined RC Columns (G0S0T0 and G0S1T0)

For the RC column, the lateral load-displacement curve was almost linear at the initial stage of loading. At the second cycle of the same target deformation, the stiffness and lateral load-bearing capacity of the specimen hardly degraded. However, the residual deformation became larger and the unloading stiffness and bearing capacity decreased with the increase of the lateral displacement, but the pinch contraction phenomenon of the hysteresis hoops was not obvious. When the displacement was 24 mm, the test was stopped due to the large area of concrete spalling. At this moment, the lateral load was 73.4% of the axial peak load of the column. For specimen G0S1T0, the residual deformation during unloading was small at the beginning. The stiffness and the bearing capacity of the specimen at the early stage did not significantly decrease at the same deformation level. The hysteretic pinch phenomenon was also not obvious in this column, demonstrating that it had a strong energy dissipation capacity (Fig. 6). When the lateral displacement was 72 mm, the lateral load decreased to 62% of the peak load.

FRP–Steel-Confined RC Columns (G5S1T0, G7S1T0, and C7S1T0)

For specimen G5S1T0, the lateral load and stiffness of the specimen did not change and the residual deformation was small at the initial stage. However, with the increase of lateral displacement, the hysteresis loop developed an obvious pinch and shrink phenomenon, but the shape of the loop was still fat (Fig. 6). The bearing capacity of the column did not decrease rapidly after reaching the peak load, indicating that the ductility of the column was satisfactory. For specimen G7S1T0, the shape and variation of the hysteresis curve were very similar to those of G5S1T0; however, the hysteresis loop of the G7S1T0 was fatter. For Specimen C7S1T0, the residual deformation was small, and the stiffness and bearing capacity had almost no degradation when the displacement was small. As the displacement increased, the residual deformation of the specimen increased, and the stiffness and bearing capacity decreased obviously.

FRP–Steel-Confined SRC Columns (G0S1T1, G5S1T1, and G7S1T1)

Specimen G0S1T1 had a fusiform hysteresis loop at the initial stage, and the hysteresis curve became gradually fatter with the increase of the displacement and showed no sign of pinch-and-shrink phenomenon (Fig. 6). This demonstrates that the column possessed excellent energy dissipation ability. For Specimen G5S1T1, the bearing capacity and stiffness did not significantly change under the same displacement. With the increase of loading, the shape of the hysteresis loop tended to become fatter. The degradation rate of the lateral load was small after the column reached its peak load, meaning that the column had satisfactory ductility. For Specimen G7S1T1, the residual deformation of the column during the initial loading was quite small. Similar to G5S1T1, no obvious degradation occurred in the stiffness and lateral load of the specimen at the same level of lateral displacement. With the increase of lateral displacement, the hysteresis curve of the specimen became fatter, showing its strong energy dissipation capacity. Comparing G7S1T1 and G5S1T1, no significant difference was observed in G7S1T1, indicating that increasing the number of GFRP layers had no influence on the seismic performance of the SRC columns.

Strain Evolution of Reinforcing Rebars and Steel Tube

Fig. 7 demonstrates that when the lateral load increased, the strain of the steel rebars increased with the lateral displacement of the RC column and steel tube–confined RC columns. When the displacement was 32 mm, the longitudinal reinforcement in L2 had a strain higher than its yielding strain, i.e., 2,000 $\mu\varepsilon$. With the increase of the lateral displacement, the longitudinal reinforcement began to yield. However, the maximum compression strain of the longitudinal reinforcement reached 2,500 $\mu\varepsilon$ at the later loading stage, indicating that it did not undergo significant plastic deformation. Fig. 7 shows that the stirrups confined the concrete well in the circular RC column.

Taking Specimen G7S1T0 as an example with the FRP–steel-confined RC columns, the maximum strains of the steel tube at the top of the base beam in both sides were 6,602 and 3,543 $\mu\varepsilon$, both of which exceeded the yielding strain of the tube (Fig. 7). The hoop strain on the outside tube confirmed that the steel tube was in tensile strain. Similar to the variation law of longitudinal strain, the amplitudes of HN50 and HS50 close to the top of the base beam were 4,883 and 4,883 $\mu\varepsilon$, respectively. Specimen G0S1T1 had a similar strain evolution to that of Specimen G7S1T0. For FRP–steel-confined SRC Column G5S1T1, the strains of LN50 and LS50 near the base beam were 6,823 and 5,949 $\mu\varepsilon$, respectively. All the results of strain gauges indicated that the steel hoops were under tension. This was due to the expansion of the core concrete after multiple lateral reserved loads, leading to an increase in the deformation of steel tube confined by the GFRP sheets. At the same time, the strains in HN50 and HS50 located on the south and north sides were 6,755 and 4,799 $\mu\varepsilon$, respectively, which reached yielding status. In summary, in the FRP–steel-confined SRC columns, at the same section of the column foot, the strains on the north side, the south side, and the neutral axis were all different, which means that the hoop strain distribution was not uniform. The strain of the steel tube in the confined SRC columns was smaller than that of other specimens because the sectional rigidity of the SRC column was quite large due to the use of H-section steel.

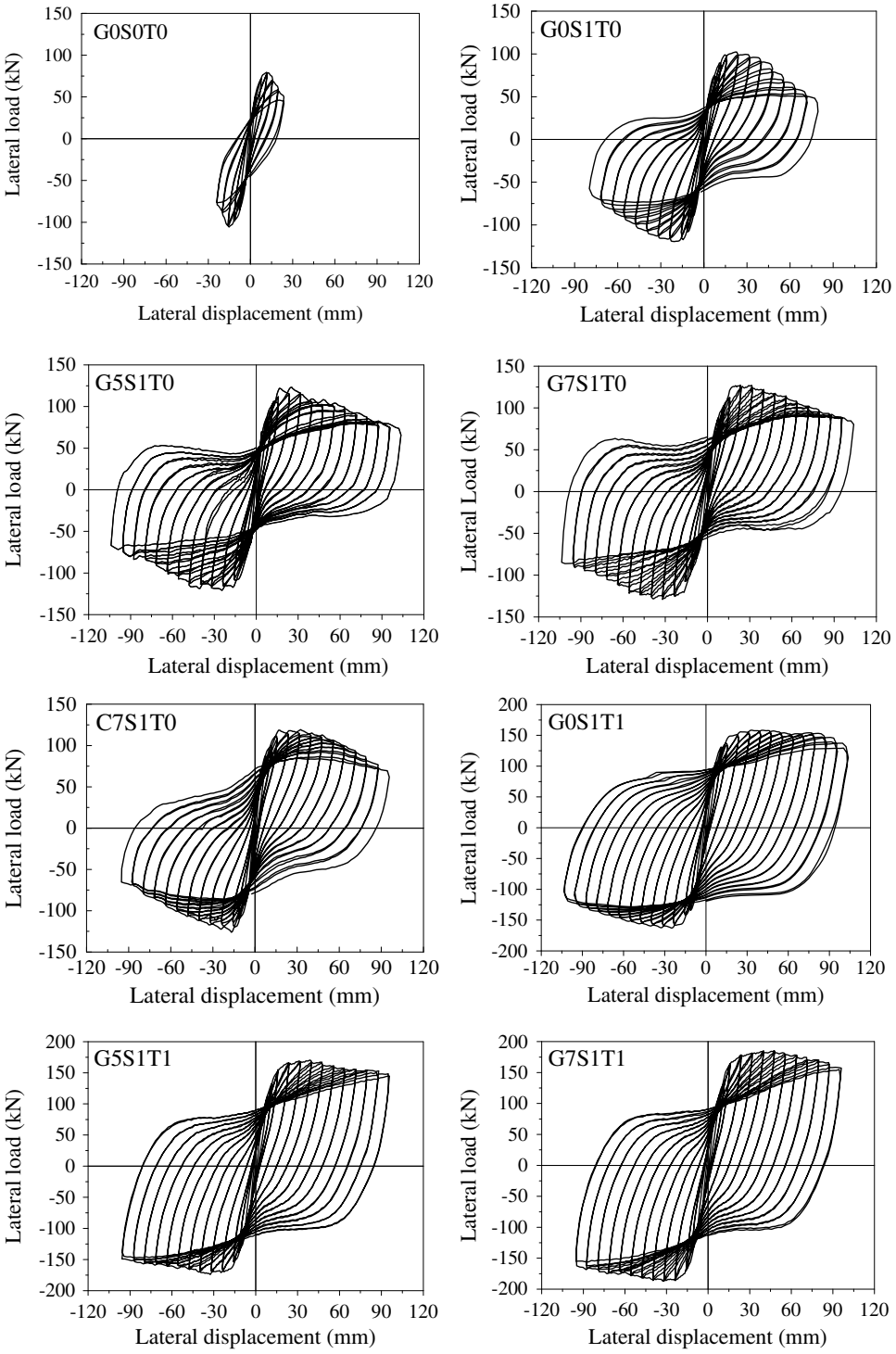

Fig. 6. Hysteresis behavior of the specimens.

Comparison and Analyses

Comparison of Hysteresis Behavior

Fig. 8 compares the hysteresis curves of all the tested specimens. Results show that the bearing capacity and ductility behavior of Specimen G0S1T0 was better than that of Specimen G0S0T0 owing to the external lateral confinement of steel tube. Compared with Specimen G0S1T0, an overall improved bearing capacity, ductility, and energy dissipation capacity of the steel tube–confined RC column was obtained by the GFRP wrapping, such as in Specimens G5S1T0 and G7S1T0. Furthermore, with the increase of the number of layers of FRP sheet, the enhancement effect of GFRP wrapping was more obvious.

Examining the case of Specimens G5S1T0 and G7S1T0, the seismic performance of the FRP–steel-confined RC columns improved as the number of layers of FRP sheet increased, but the enhancement effectiveness decreased as the number of FRP layers increased. For Specimens G7S1T0 and C7S1T0, although the lateral confinement (both the lateral confinement stiffness

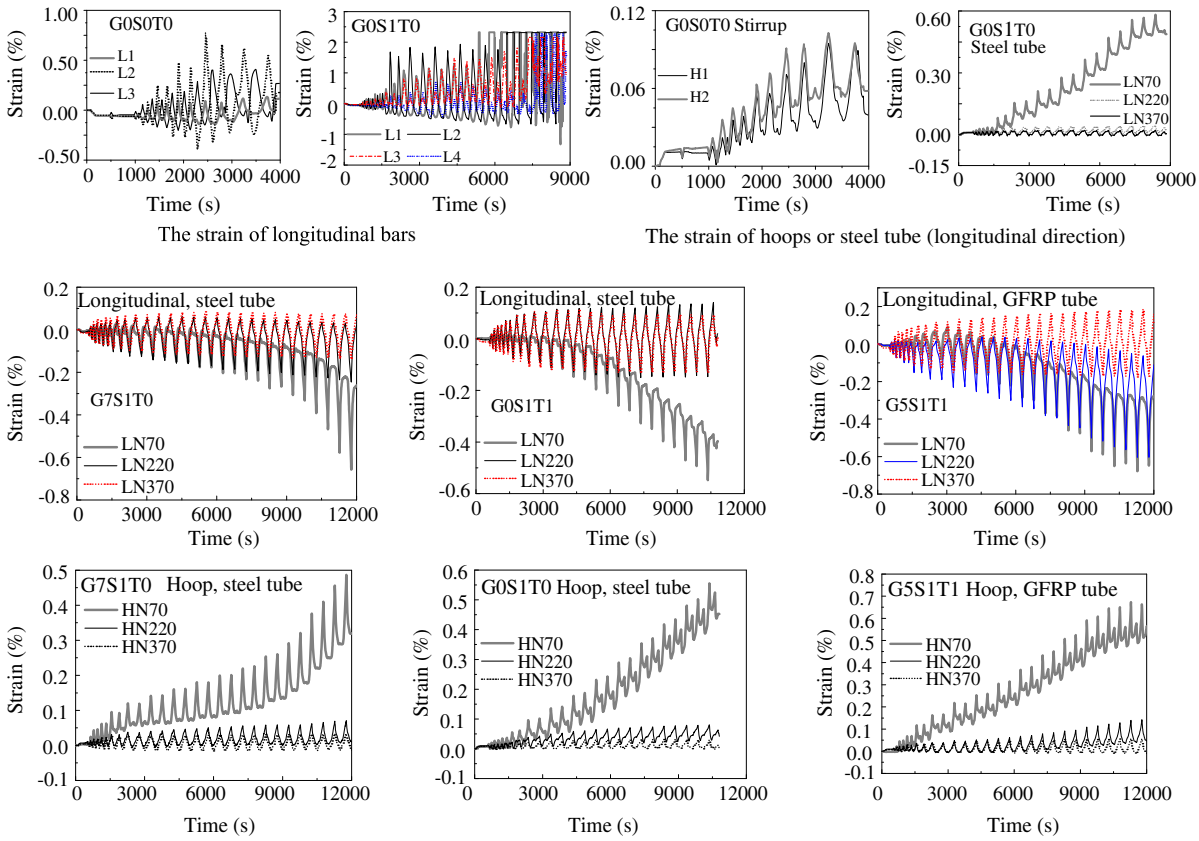

Fig. 7. Strain evolution of reinforcing bars and steel tube.

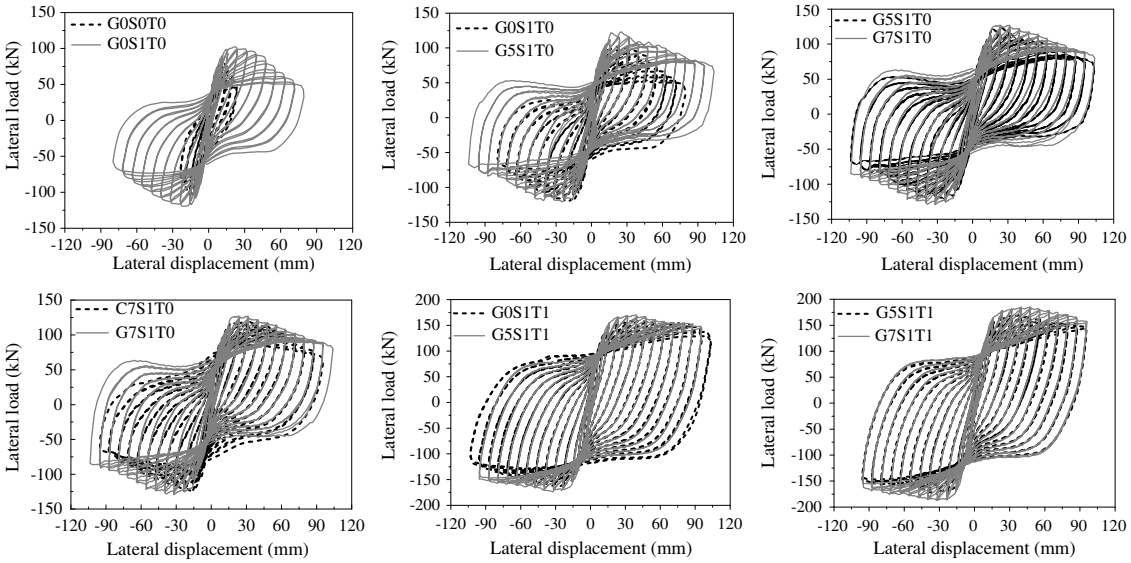

Fig. 8. Comparison of experimental load-displacement curves.

and strength) of the CFRP was stronger than that of the GFRP, the load-carrying of Specimen G7S1T0 was slightly better than that of Specimen C7S1T0. This can be explained as follows: (1) the failure mode of the confined RC columns was controlled by the damages and cracks in the confined RC, but not controlled by the rupture of the FRP wrapping which usually occurs in axial compressive columns, which indicated that the FRP material was not fully utilized; and (2) this abnormal case may have been induced by manufacturing errors of the specimens, testing errors, and so forth.

For GFRP–steel-confined RC/SRC columns, the bearing and deformation capacities of Specimen G5S1T1 (or G5S1T0) improved when using GFRP to confine steel tube, compared with those of Specimen G0S1T1 (or G0S1T0). This indicates that the FRP–steel composite tube can improve the seismic performance of RC/SRC columns in an effective manner. However, when the

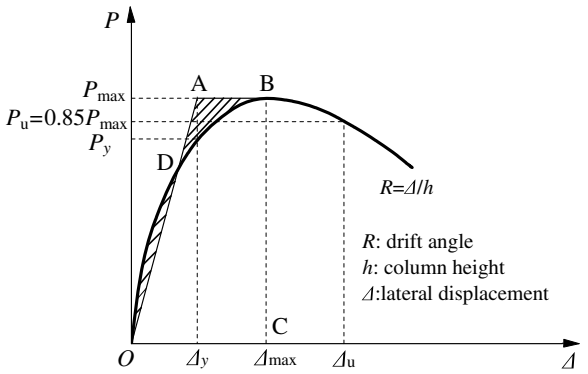

Fig. 9. Ductility calculation method: the equivalent elastoplastic energy absorption method according to Park (1988).

amount of steel reinforcement (H-section steel, steel reinforcing bars, and steel tube) was high, the improvement caused by FRP wrapping became not obvious. For Specimens G5S1T1 and G7S1T1, the increase of the number of layers of FRP did not significantly improve the shear resistance and the deformation capacity of the confined SRC columns. This could be because the confined columns using H-section steel already had high seismic performance, indicating that the confinement effectiveness of the FRP sheets was not developed.

Skeleton Curves—Deformation and Ductility

Skeleton curves can clearly reflect the bearing capacity and ductility of RC members which are the main considerations of the seismic design of the members. Generally, a skeleton curve mainly includes three characteristic points: yield strength point, peak strength point, and ultimate strength point. The peak point is the peak load of the columns, P_{max}. For the FRP–steel-confined RC columns, the ultimate point, P_u, was the point at 85% of the peak load (85% P_{max}). The deformability of FRP–steel-confined SRC columns was excellent; however, the ultimate deformation was large when the lateral load decrease was not obvious. For safety reasons, all tests were stopped before reaching the ultimate state of the columns. For a comparative analysis, the ultimate strength points of two FRP–steel-confined SRC columns (Specimens G5S1T1 and G7S1T1) were considered as the point at which the lateral load decreased to 90% of the peak load in this study.

There is no uniform calculation method to adjust the yield point of the concrete element. In this paper, the equivalent elastoplastic energy absorption method (Park 1988) was applied to define the yielding point by introducing an additional line in the load-deformation curve to define an equivalent elastoplastic displacement with the same energy dissipation (Fig. 9): the trapezoidal OABC area is equal to the area bounded by the curve ODBCO. In Fig. 9, Δ_u and P_u represent the ultimate displacement and the ultimate load, respectively; P_y and Δ_y are the yield load and displacement, respectively; and P_{max} is the peak load and Δ_{max} is the corresponding displacement. Here, P_u was taken as 85%P_{max} or 90%P_{max} for columns with and without H-section steel, respectively, with the exception of Specimen G0S1T1 (85%P_{max}); R is the drift angle of the columns.

Fig. 10 compares the skeleton curves of all the tested specimens, and Table 3 summarizes the test results. The yield loads of FRP–steel-confined RC columns without H-section steel increased slightly with the number of layers of FRP wrapping. The yield displacement for the steel tube–confined or FRP–steel-confined RC columns was larger than that of RC columns. Compared with Specimen G0S1T0, Specimens G5S1T0 and G7S1T0 had a larger yield load, which increased by 5.6% and 11.0%, respectively. The peak loads of the specimens G5S1T0 and G7S1T0 increased by 10.2% and 16.0%, respectively, whereas their peak displacements increased by 14.9% and 28.4%, respectively, and their ductility coefficients increased by only 0.5% and 3.1%, respectively. This indicates that the ultimate shear capacity and deformation capacity of the steel tube–confined RC column significantly improved after confinement by FRP wrapping, whereas no significant improvement was achieved in its ductility. On the other hand, the CFRP–steel-confined specimen (C7S1T0) had a better ductile coefficient, which was higher than that of the GFRP–steel-confined specimen (G7S1T0) because the confinement of the CFRP was stronger than that of the GFRP; the same number of layers of FRP was used.

For the specimens using H-section steel, similar results were obtained. Compared with Specimen G0S1T1, with an increase of the number of GFRP layers, the yielding load of Specimens G5S1T1 and G7S1T1 increased slightly by 0.3% and 10.2%, their peak load increased by 8.8% and 17.9%, and their ultimate displacement increased by 7.1% and 12.9%, respectively. Meanwhile, the ductility coefficients of G5S1T1 and the G7S1T1 also increased slightly with increasing number of GFRP layers.

Stiffness Degradation

The lateral stiffness of RC columns generally degrades under a reversed cyclic loading for several reasons, such as the decrease of effective compression area of columns caused by concrete cracking, yielding of steel reinforcement, and so forth. Stiffness in this study refers to an equivalent lateral stiffness, which is the average

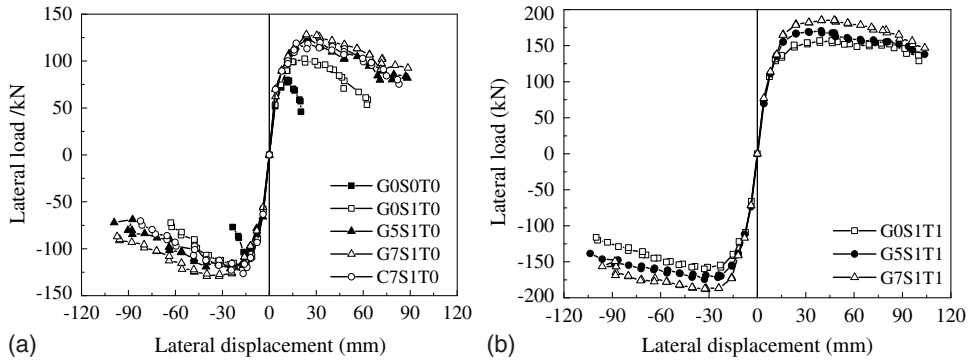

Fig. 10. Experimental load-displacement skeleton curves: (a) without H-steel; and (b) with H-steel.

Table 3. Summary of test results of test specimens

Specimen	P_y	Δ_y (mm)	P_{max} (kN)	Δ_{max} (mm)	P_u (kN)	Δ_u (mm)	R (%)	μ_Δ
G0S0T0	80.55	8.30	92.95	13.42	79.01	16.44	1.37	1.98
G0S1T0	96.44	10.49	110.95	21.68	94.30	43.90	3.66	4.19
G5S1T0	101.84	12.37	122.29	24.91	103.95	52.11	4.34	4.21
G7S1T0	107.01	14.53	128.72	27.83	109.41	62.70	5.23	4.32
C7S1T0	103.81	11.52	122.97	24.60	104.53	51.37	4.28	4.46
G0S1T1	149.83	13.99	158.45	35.79	134.68	72.64	6.05	5.19
G5S1T1	150.34	14.78	172.46	36.22	155.22	77.81	6.48	5.26
G7S1T1	165.07	15.47	186.78	39.75	168.10	81.99	6.83	5.30

Note: μ_Δ = displacement ductility coefficient, Δ_u/Δ_y.

value of the load-displacement ratios at the unloading points in the positive and negative directions of the first loading hoop of each target displacement level. Fig. 11 demonstrates the stiffness degradation curve of all specimens. Results show that the initial stiffness of the RC column (G0S0T0) was low, whereas members confined by a steel tube or FRP–steel tube had a much higher stiffness. As the lateral displacement increased, the stiffness of the confined RC columns degraded slowly. In addition, the stiffness degraded more slowly when the number of GFRP layers increased. The initial stiffness of Specimens G0S1T1, G5S1T1, and G7S1T1 was almost the same because all SRC columns had a strong stiffness. As the lateral displacement increased continuously, the degradation rates of the lateral stiffness of the SRC specimens remained almost identical.

Energy Dissipation Capacity

The energy dissipation capacity of RC elements is an important index to evaluate their capacity to absorb earthquake energy induced by ground shaking. RC structures could fail and collapse due to poor energy dissipation during an earthquake. In this study, the cumulative energy dissipation was calculated considering only the first load hoop at the corresponding displacement level. The accumulated energy dissipation of RC columns was less than that of the confined RC columns at the same lateral displacement (Fig. 12). As the number of GFRP layers increased, the energy dissipation capacity of the confined columns increased. However, the accumulated energy dissipation of G7S1T0 was only slightly higher than that of G5S1T0. This was because Specimen G5S1T0, wrapped with five layers of GFRP may already have been overconfined. Therefore, the effect of increasing GFRP layers on energy dissipation was small in G7S1T0. Similarly, Specimen C7S1T0 had greatly improved energy dissipation capacity compared with Specimen G0S0T0, but the energy consumption capacity of Specimens G7S1T0 and G5S1T0 was almost the same.

For the SRC columns (G0S1T1, G5S1T1, and G7S1T1), similar behavior was obtained: (1) in the initial stage, the accumulated

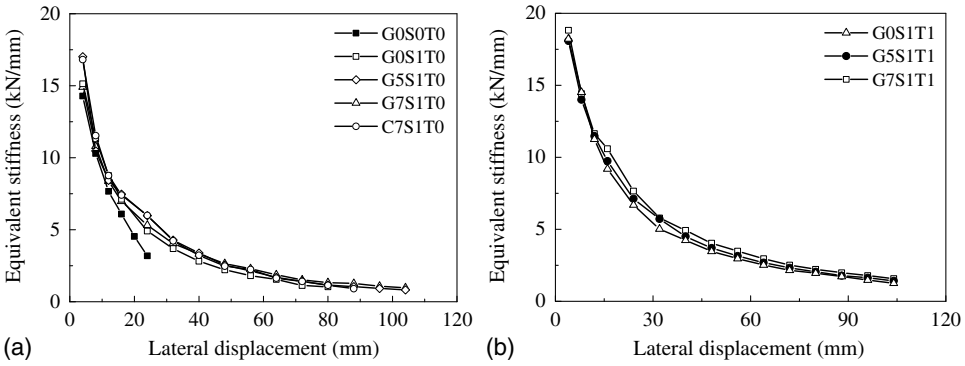

Fig. 11. Evolution of the equivalent stiffness of test specimens: (a) without H-steel; and (b) with H-steel.

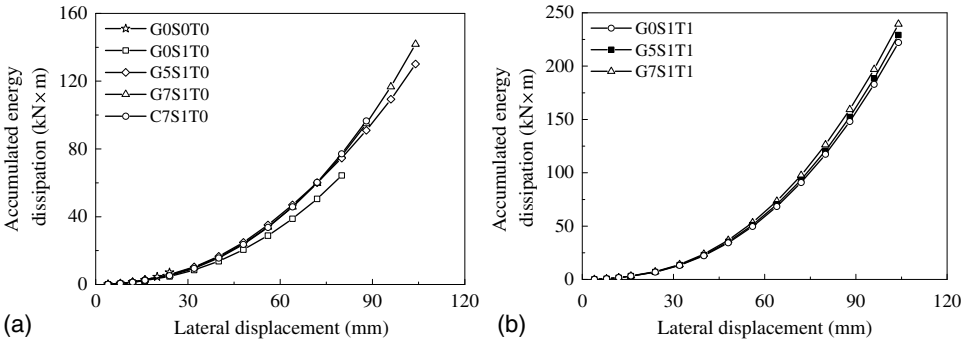

Fig. 12. Accumulated energy dissipation of test specimens: (a) without H-steel; and (b) with H-steel.

J. Struct. Eng., 2019, 145(9): 04019085

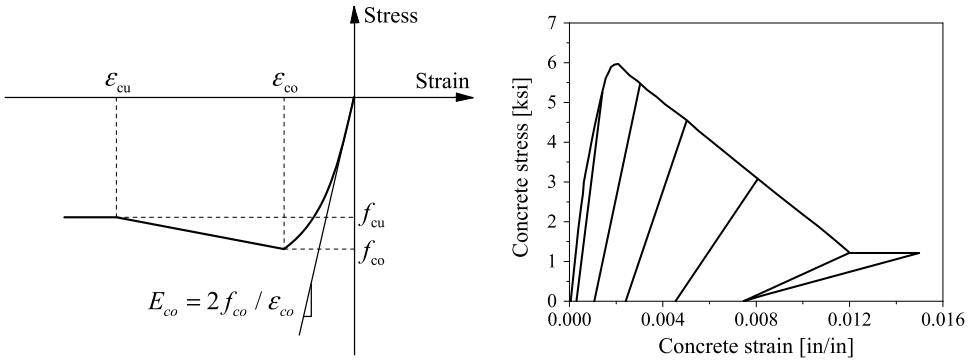

Fig. 13. Stress-strain models of Concrete01 in OpenSees according to Mazzoni et al. (2006).

energy dissipation of the specimens was similar for all specimens; (2) as the lateral displacement increased, the energy dissipation capacity of the columns increased, had a different evolution, and ultimately the energy consumption of G7S1T1 was highest; and (3) the number of GFRP layers had no significant influence on the energy dissipation capacity of the SRC columns. This again shows that the improvement of the seismic performance of the SRC columns due to an increasing the number of layers of GFRP sheet was relatively small.

FEM Simulation of FRP–Steel-Confined RC Columns

According to section "Comparison and Analyses," the GFRP wrapping did nothave a positive effect on the seismic performance of the SRC columns. The main reason could be that the core SRC column already possessed a high stiffness to the lateral deformation under the reversed cyclic loads. Therefore, this section emphasizes the simulation of FRP–steel-confined RC columns. OpenSees version 2.5.0, an open-source object-oriented software, was used for the analysis of the tested RC and FRP–steel-confined RC columns. The basic assumptions for the analyses of the columns included: (1) concrete section remained a plane and normal to the neutral axis after bending; (2) the slippage between steel rebar and concrete was neglected to simplify the simulation; and (3) the shear effect was neglected to simplify the simulation because the shear span ratios of all columns in this FEM were not less than 2 (it was 4 for most cases), which indicated the flexural failure mode occurred in the columns and the shear effect was relatively small. This section discusses the geometric and materials models used in the program.

Material Model and Cross-Section Rule

Concrete and Steel Tube–Confined Concrete

For the RC column, a three-line constitutive model proposed first by Kent and Park (1971) and modified by Scott et al. (1982) was selected as a backbone curve for concrete material. The backbone and hysteresis model of concrete (uniaxial materials of Concrete01 in OpenSees) are presented in Fig. 13 (Mazzoni et al. 2006). The related equations of the model are as follows:

$$f = \begin{cases} Kf_{co}\left[2\left(\frac{\varepsilon}{\varepsilon_{cc}}\right) - \left(\frac{\varepsilon}{\varepsilon_{cc}}\right)^2\right], & \varepsilon \le \varepsilon_{cc} \\ Kf_{co}\left[1 - Z\left(\frac{\varepsilon}{\varepsilon_{cc}}\right)\right], & \varepsilon_{cc} \le \varepsilon \le \varepsilon_{cu} \\ 0.2Kf_{co}, & \varepsilon \ge \varepsilon_{cu} \end{cases} \quad (1)$$

where

$$K = 1 + \rho_v f_{yh}/f_{co} \quad (2)$$

$$Z = \frac{0.5}{\frac{3+0.29f_{co}}{145f_{co}-1000} + 0.75\rho_v\sqrt{\frac{b}{s}} - 0.002K} \quad (3)$$

ε_{cc} = strain corresponding to the peak stress of the confined concrete, taken as 0.002 K; K = coefficient of the increase of the peak load caused by the confinement; Z = slope of the strain decrease curve; f_{co} = compressive strength of standard nonconfined concrete cylinders; f_{yh} = yield strength of stirrups; ρ_v = volumetric reinforcement ratio of stirrups; b = width of core concrete; and s = spacing of stirrups. For steel tube–confined RC columns, the analysis of the confined concrete of the columns adopted the constitutive model of steel tube–confined concrete proposed by Lin (2012).

FRP–Steel-Confined Concrete Model

Monotonic Model. An analysis-oriented stress-strain model for FRP-steel-confined concrete was used in this paper. In analysis-oriented models for FRP-confined concrete (Jiang and Teng 2007), a passive confining stress-strain model for FRP-confined concrete in FRP–steel-confined concrete columns can be achieved from an active confining model for concrete through an incremental approach. The model is proposed on the assumption that the axial stress and strain of FRP–confined concrete at a given hoop strain are the same as those of the same concrete confined actively with a constant confining pressure equal to that provided by the FRP wrapping (Jiang and Teng 2007). The axial stress-strain model for concrete developed by Popovics (1973) was adopted in this paper. Popovics (1973) proposed a stress-strain model for confined concrete with active confining, which presents great analysis accuracy. Thus, it is suggested that this model be used to analyze the stress-strain of GFRP–steel-confined concrete elements, which is

$$\frac{\sigma_c}{f_{co}} = \frac{(\varepsilon_c/\varepsilon_{cc}) \cdot r}{r - 1 + (\varepsilon_c/\varepsilon_{cc})^r} \quad (4)$$

$$r = \frac{E_c}{E_c - f_{cc}/\varepsilon_{cc}} \quad (5)$$

Based on the research conducted by the research group of the first author of the paper (Lin 2012; Ran 2014; Huang 2016), it is suggested that the active (stirrups and steel tube) and passive confining actions (FRP wrapping) in FRP–steel-confined concrete columns be considered to model the peak axial stress and the

corresponding axial strain of FRP–steel-confined concrete. The proposed models are expressed

$$\frac{f_{cc}}{f_{co}} = 1 + 4.08\left(\frac{f_{lf}}{f_{co}}\right)^{1.28} + 5.5\left(\frac{f_{ls}+f_{lh}}{f_{co}}\right)^{0.86} \quad (6)$$

$$\frac{\varepsilon_{cc}}{\varepsilon_{co}} = 2 + 11.72\left(\frac{f_{lf}}{f_{co}}\right)^{0.55} + 5.8\left(\frac{f_{ls}+f_{lh}}{f_{co}}\right) \quad (7)$$

Referring to the confining mechanism of FRP-confined CFST elements proposed by Hu (2011), in this study, the relationship between hoop strain (ε_h) and axial strain of confined concrete is calculated as

$$\frac{\varepsilon_{cc}}{\varepsilon_{co}} + 0.66\left(1 + 8\frac{f_l}{f_{co}}\right) \times \left\{\left[1 + 0.75\left(\frac{\varepsilon_h}{\varepsilon_{co}}\right)\right]^{0.7} - \exp\left[-7\left(\frac{\varepsilon_h}{\varepsilon_{co}}\right)\right]\right\} = 0 \quad (8)$$

where f_{cc} = compressive stress of confined concrete; f_{ls}, f_{lf}, and f_{lh} = confining stresses of steel tube, FRP, and stirrups, respectively; f_l = total confining pressure; E_c = elastic modulus of concrete, which is taken as $4{,}736f_{co}^{0.5}$; ε_{cc} = axial strain of confined concrete at its strength; σ_c = axial stress of the tested concrete specimen; ε_{co} = axial strain of concrete corresponding to its compressive strength; and ε_c = unit strain of concrete corresponding to σ_c.

As an analysis-oriented stress-strain model, the generation of the axial stress-strain curves for FRP–steel-confined concrete is achieved by an incremental process (Huang 2016).

Multicycle Model. The cyclic constitutive model includes mainly the skeleton model and hysteretic law. The latter includes two key unloading and reloading paths, and the calculation of plastic strain and stress degradation. Here, the monotonic model proposed previously was used to simulate the skeleton curve of the FRP–steel-confined RC columns under cyclic loading. For the hysteretic models, because the strength ratio of the FRP materials to steel was fairly large, the confining effectiveness of the FRP–steel tube on the concrete was considered to be similar to that of the FRP-confined concrete. Meanwhile, due to the existence of the steel tube and transverse rebars in the FRP–steel-confined RC columns, the authors suggest using the improved model proposed by Lam and Teng (2009). The key features and related equations are presented in Fig. 14. The details of the multicyclic model were given by Huang (2016).

New Material Constitutive Model for FRP–Steel-Confined Concrete Developed with OpenSees Programming

An accurate material constitutive model is the base of the analysis of the RC columns subjected to reversed cyclic loads. OpenSees is a well-known open-source platform with a strong nonlinear structural analysis and high compatibility. FRP–steel-confined concrete can significantly improve the seismic behavior of the RC columns, as demonstrated in section "Comparison and Analyses." However, the existing material constitutive models for FRP–steel-confined concrete are not available in the current version of OpenSees. Using the C++ programming language, a new user-defined material constitutive model based on the monotonic and multicycle constitutive model proposed in section "FRP–Steel-Confined Concrete Model" was developed and applied in an OpenSees platform. The developed new material constitutive model is suitable for FRP–steel-confined concrete with a circular section. The material models and elements are separate and independent in OpenSees. Therefore, all existing elements in OpenSees are compatible with the new material model. Compared with the existing concrete model, the new material model can accurately simulate the true stress-strain relationship of FRP–steel-confined concrete, especially the unloading rules including residual strain, which improves the pinching effect of FRP–steel-confined RC columns.

Steel Model

This study used a constitutive model of steel reinforcement proposed by Menegotto and Pinto (1973) considering steel reinforcement as an elastic-perfectly plastic material, which is given as

$$\sigma^* = b\varepsilon^* + \frac{(1-b)\varepsilon^*}{(1+\varepsilon^{*R})^{1/R}} \quad (9)$$

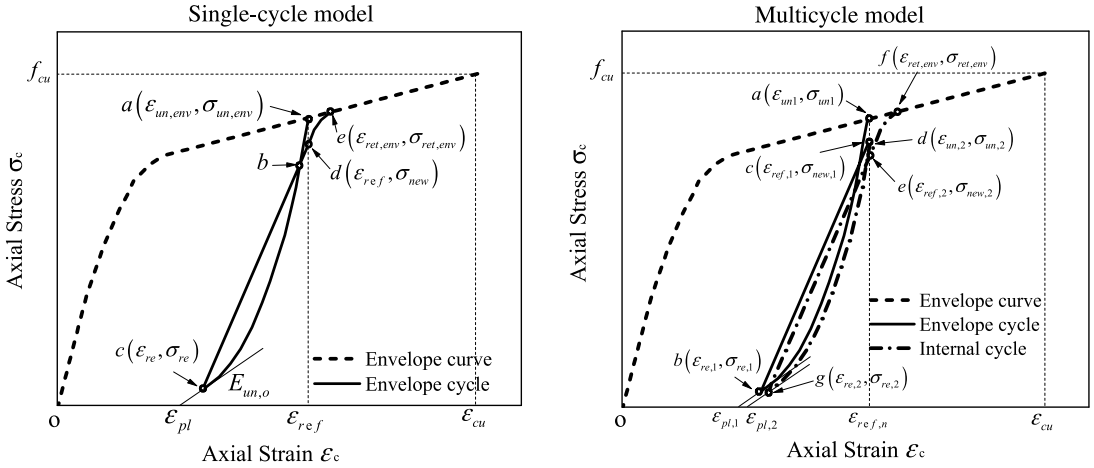

$$\varepsilon_{pl,n} = \begin{cases} 0 & 0.0 < \varepsilon_{un,env} \le 0.001 & n=1 \\ k_s[1.4(0.87-0.004f_{co}')-0.64](\varepsilon_{un,env}-0.001) & 0.001 < \varepsilon_{un,env} \le 0.0035 & n=1 \\ (0.87-0.004f_{co}')\varepsilon_{un,env} - k_6 & 0.0035 < \varepsilon_{un,env} \le \varepsilon_{cu} & n=1 \\ (1-\omega_n)\varepsilon_{un,n} + \omega_n\varepsilon_{pl,n-1} & & n \ge 2 \end{cases}$$

$$\gamma_{re,n} = \frac{\varepsilon_{un,n+1}-\varepsilon_{pl,n}}{\varepsilon_{ref,n}-\varepsilon_{pl,n}} \qquad \sigma_{new,n} = \varphi_n\sigma_{ref,n}$$

$$\sigma_c = a\varepsilon_{x,c}^{\eta} + b\varepsilon_{x,c} + c \qquad \eta = 350\varepsilon_{un} + 3$$

Fig. 14. Key parameters of proposed cyclic constitutive models according to Huang (2016).

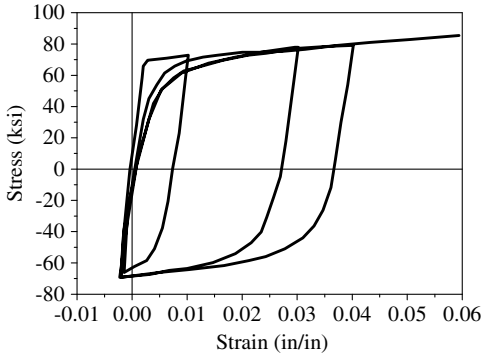

Fig. 15. Hysteretic property of Steel02 model in OpenSees.

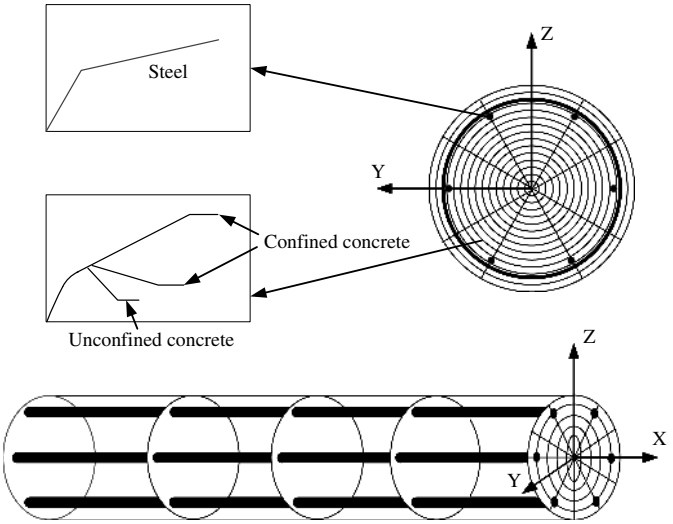

Fig. 16. Schematic representation of the fiber's cross section.

where b = strain hardening coefficient; σ^* and ε^* = normalized stress and strain, respectively; and R = curvature parameter. The detailed calculations of the parameters were given by Menegotto and Pinto (1973) and Orakcal et al. (2006). Fig. 15 depicts a typical hysteretic stress–strain response output for steel reinforcement.

Cross-Section Rule

A distributed-plasticity, force-based nonlinear beam–column element was selected for the analysis of all columns. For FRP–steel-confined RC columns, two beam–column elements were used to simulate the FRP-confined hinge zone of 500 mm height and the remaining part of the column, respectively, which was described in section "Test Overview." Similarly, two beam–column elements with the same element size were used for RC columns and steel tube–confined RC columns. A cantilever half-column model was used in this simulation, which was used to as a test. As described in section "Test Overview," the steel tubes and the FRP wrapping were terminated at their two ends to avoid direct axial compression. Therefore, the steel tube and the FRP wrapping in the confined RC columns mainly provided the confining effect for the concrete core. To simply the simulation, the models of the stirrup, the steel tube, and the FRP wrapping in the confined RC columns were not built in this paper, whereas the confining effects of the three parts on the concrete core were considered by introducing the proposed stress-strain relationship of FRP–steel-confined RC into the element (Fig. 16). The circular cross section of all columns was divided into 36 parts in the hoop direction and 30 parts in the radial direction. Therefore, 1,080 fibers were used. The 1,080 fibers (36×30 fibers) were determined to balance computational accuracy and computational efficiency before ensuring convergence. However, a convergence study regarding the element size and number of fibers was not conducted.

FEM Model Validation

Fig. 17 compares the simulated and tested results of RC columns and FRP–steel-confined RC columns. The peak loads of the simulated curves were very similar to their measured values, and the corresponding lateral displacements were also consistent with the test results. For the FRP–steel-confined RC columns, the simulated curves were in good agreement with their experimental curves. Although a new material constitutive model for FRP–steel-confined concrete, which improved the pinching effect of the columns, was implemented in the analysis, the pinching effect of the simulated curves was still more obvious than that of the test curves, especially for Specimens G5S1T0, G7S1T0, and C7S1T0. This may be due to the fact that the slippage of steel rebar and concrete was not considered, which was neglected to simplify the simulation in this paper. Overall, the simulation results were in good agreement with the experimental results. Therefore, it is feasible to use the OpenSees-based FEM model to simulate the seismic performance of FRP–steel-confined RC columns.

Parametric Study of FRP–Steel-Confined RC Columns

For the proper seismic design of FRP–steel-confined RC columns, it is necessary to understand the influence of main parameters on the seismic performance of the columns to make reliable adjustments accordingly based on laboratory study. In this study, a parametric study was carried out of the effects of various parameters on the seismic preformation of FRP–steel-confined RC columns. The basic models from the preceding simulation program were used. The main structural parameters studied were axial load ratio (0.1–0.8), shear span ratio (2–10), steel tube thickness (1–6 mm), longitudinal steel ratio (change steel diameter), number of FRP layers (1–8 layers), and wrapping height of FRP sheet on the columns (0–1,000 mm).

Effect of Axial Load Ratio

Based on the tested Specimens G0S1T0 and G5S1T0, the axial load ratio ranged from 0.1 to 0.8 (Fig. 18), and the results demonstrated that during the increase of axial load, the bearing capacity of the specimens under reversed cyclic loads increased. However, the bearing capacity of the specimens decreased with an increase of axial load more rapidly in the postpeak stage. This shows that the ductility decreased as the axial load ratio increased. Specimen G5S1T0, confined by five layers of GFRP sheet had better ductility than did Specimen G0S1T0, confined only by the steel tube.

Effect of Shear Span Ratio

Fig. 19 demonstrates the impact of shear span ratio on the seismic behavior of Specimens G0S1T0 and G5S1T0 without changing the other conditions. The effect of the shear span ratio was basically the same when different types of external lateral confinement were used. As the shear span ratios increased, the bearing capacity of the specimens decreased in turn. The peak displacement also increased when shear span ratio increased, meaning that the flexural capacity of the columns was stronger.

Effect of Thickness of Steel Tube

Fig. 20 shows the results when the thickness of steel tube increased from 1 to 6 mm in Specimens G0S1T0 and G5S1T0. As the

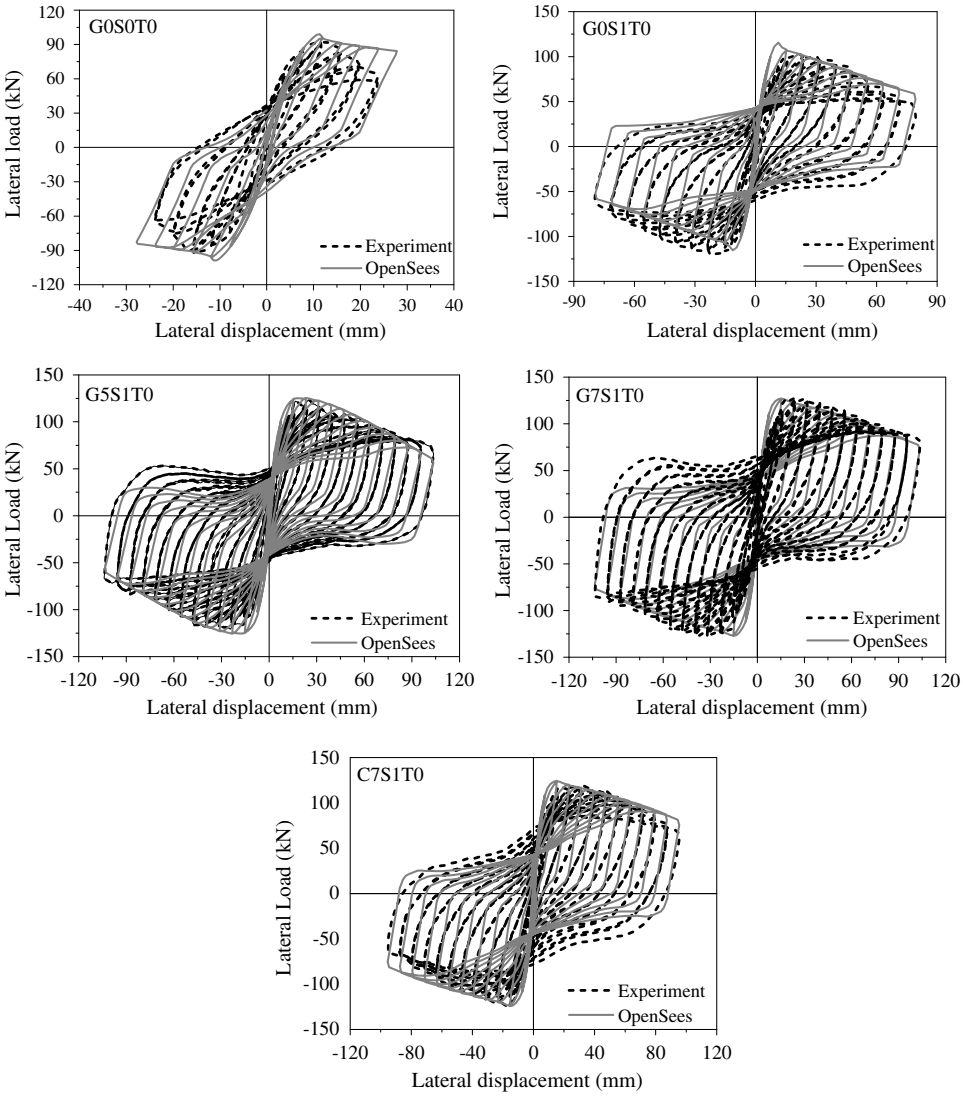

Fig. 17. Comparison of simulation and test results of circular RC and confined RC columns.

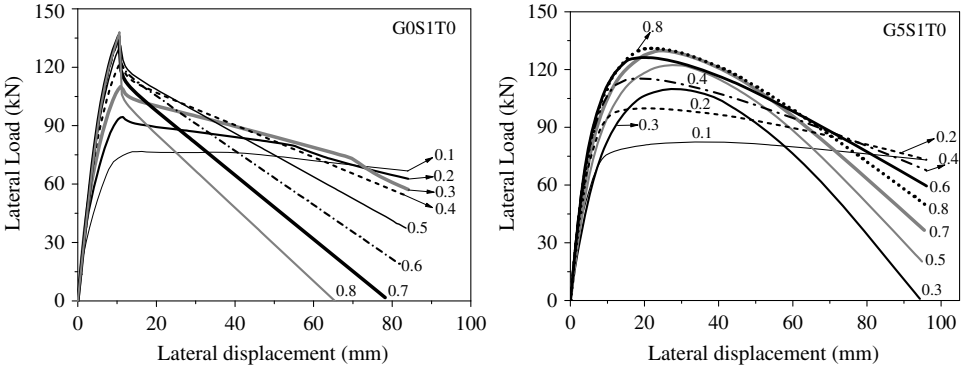

Fig. 18. Influence of axial load ratio on FRP–steel-confined RC columns.

thickness of steel tube increased, the ductility and load carrying capacities of the specimens were improved. Moreover, changing the thickness of steel tube had a greater influence on Specimen G0S1T0, because its bearing capacity and ductility improved more significantly, and its peak strain increased. On the other hand, because the lateral confinement of five layers of GFRP sheet was considered to be overconfining, the effect of the thickness of the steel tube on Specimen G5S1T0 was not very significant. When using FRP–steel tube to confine RC columns in practice, it is not advisable to increase the thickness of steel tube in order to increase

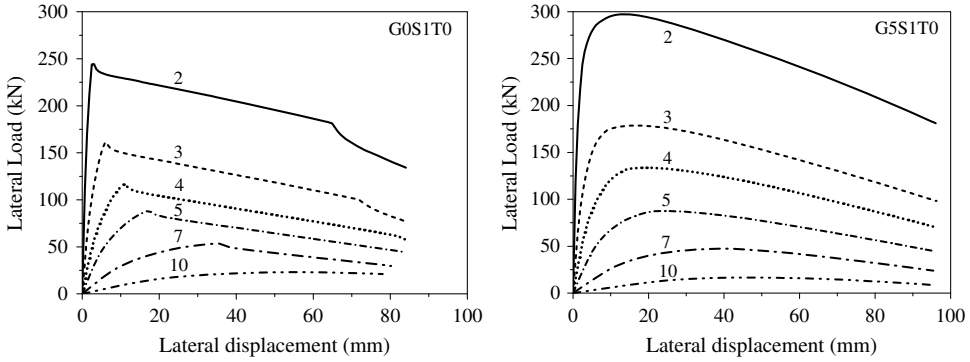

Fig. 19. Influence of shear-span ratio on FRP–steel-confined RC columns.

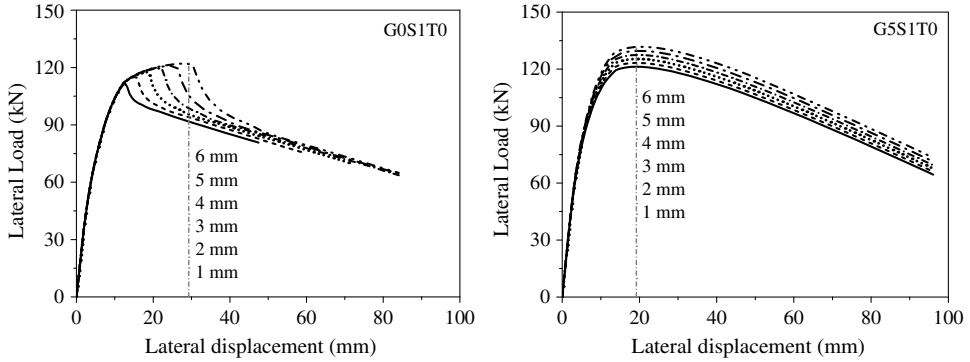

Fig. 20. Effects of steel tube thickness on FRP–steel-confined RC columns.

confinement. Simply increasing the tube thickness increases the self-weight of structures, which is not ideal for resisting the seismic actions.

Effect of Longitudinal Steel Ratio

The effect of longitudinal steel ratio on the seismic behavior of FRP–steel-confined RC columns was examined by increasing the diameter of longitudinal reinforcement (D) of the reference specimens. The results show that the bearing capacity of the two specimens improved when the reinforcement ratio of longitudinal reinforcement increased, but the influence on the degradation ratio of the lateral load of the columns in the postpeak stage was not obvious (Fig. 21).

Effect of Number of Layers and Confining Height of FRP Sheet

The effect of the number of FRP layers on the load-displacement skeleton curve of the columns is shown in Fig. 22. The lateral ultimate load and its corresponding displacement of the column increased as the number of GFRP layers increased. This indicates that as the number of GFRP layers increased, the bearing capacity and ductility of the columns increased. On the other hand, based on the results of Specimen G5S1T0, the increase of the confining height of the GFRP sheet (0, 300, 500, 800, and 1,000 mm) had no significant effect on the bearing capacity and ductility of the specimens after the height reached 300 mm. The height was more than 1.5 times the diameter of the columns, which was similar to the case of RC elements reported previously. Therefore, the confining height of circular FRP–steel-confined RC columns is suggested to be 1.5 times the column's diameter, which can achieve economical and reasonable lateral confinement.

Discussions

Plastic Hinge Region Height

The prediction of the lateral load–deformation behavior of a concrete column involves an important step, modeling the plastic hinge region (PHR) of the column (e.g., Inel and Ozmen 2006; Youssf et al. 2015; Yuan et al. 2017). The region is defined as the deformation and damage region of elements, which experiences inelastic demands. Based on the literature, previous experimental studies of concrete columns (unconfined or confined) assessed the PHR height by visually observing the damage regions at both ends of the columns (e.g., Bae and Bayrak 2008; Liu and Sheikh 2013). The damage mainly included cracks and spalling of concrete cover, which usually was considered to relate to the longitudinal plastic deformations of the columns. For FRP-confined concrete elements, Ozbakkaloglu and Sattcioglu (2006, 2007) recommended using the hoop-strain profiles of the tubes to assess the PHR height, considering an intimate relationship between the lateral expansion of FRP tube and inside damage sustained by concrete. This means that the concrete cover may be damaged with a high probability when the corresponding hoop strain of FRP tube is high at the same position. Ozbakkaloglu and Idris (2014) suggested that the PHR height can be established through a hoop distribution of the specimens at its final loading cycle. They assumed that the PHR terminated at a height where the hoop strain fell below one-third the maximum recorded strain in the cycle.

In this study, the PHR formation and propagation of the three types of tested columns, i.e., RC, confined RC, and confined SRC columns, were determined based on a combined method considering

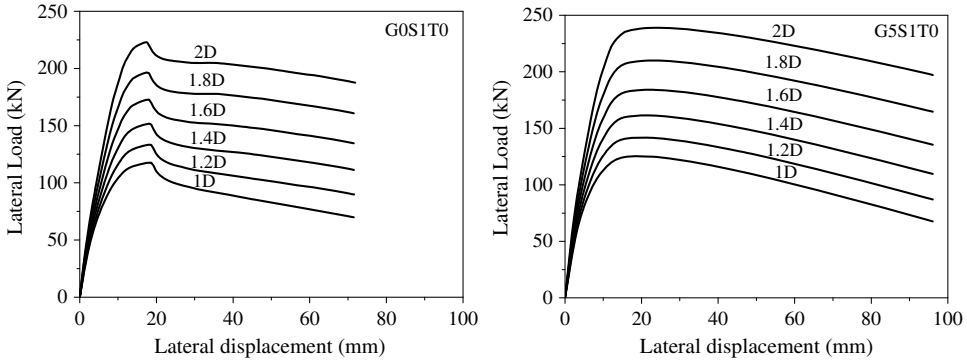

Fig. 21. Effects of longitudinal bars ratio on FRP–steel-confined RC columns.

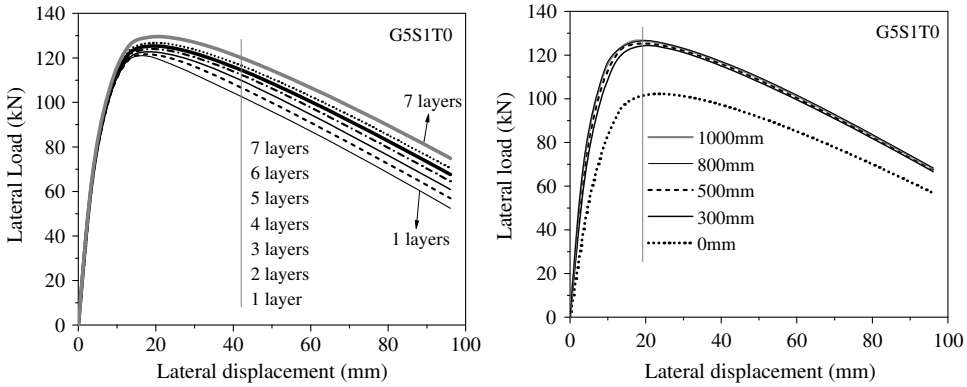

Fig. 22. Effects of confining layer number and the height of GFRP on the confined columns.

the hoop strain evolution of the FRP–steel tube and the inside cracking formation of the specimens. The average PHR height of RC column was obtained from the measured height of two sides of the column after the final load cycle. For other confined RC/SRC columns, the PHR height of steel tube–confined RC/SRC columns (G0S1T0 and G0S1T1) was determined by analyzing the hoop-strain distribution of steel tubes along their height. For the FRP–steel-confined RC/SRC columns, experimental observation and strain analyses were conducted to assess their PHR heights. The results (Figs. 5 and 7) show that the difference between the unconfined and confined columns was high, which can be mainly attributed to the different lateral confinement conditions of the columns. The lateral confinement increased the ductility and deformability of the columns, meaning that their PHR heights decreased. In addition, the strain evolutions of the steel tube–confined specimens and FRP–steel-confined specimens, such as G7S1T0, also show that the difference in the deformation capacity of the region was between 70 and 220 mm from the end of the columns. The additional confinement from the FRP material increased the deformability of the confined RC/SRC columns. The PHR height of Specimen G7S1T0 should have been between 70 and 220 mm, but it was closer to 70 mm. The damage shown in Fig. 5 verifies that the PHR height of Column G7S1T0 was about 100 mm. Compared with Specimens G7S1T0 and C7S1T0, the higher elastic modulus and tensile strength of CFRP increased the hoop strain level at 220 mm from the end of the columns. However, the hoop strains of the CFRP-steel tube at 70 and 220 mm both were quite small, which means that the PHR height was not changed significantly, and was equal to that of GFRP–steel-confined RC columns. This can also be explained by the fact that CFRP and GFRP both are very strong in tension compared with the steel tube. Within the SRC columns, there was no obvious difference between the PHR height of steel tube–confined SRC columns and FRP–steel-confined SRC columns, which both were between about 70 and 100 mm. As described previously, the H-section steel already made the RC columns strong to resist seismic action. This indicates that the additional lateral confinement of FRP materials did not affect the deformability and ductility of the columns.

Peak Drift Level of Confined RC Columns

As described previously, compared with conventional RC columns, all confined RC columns of this study had excellent seismic behavior. However, the lateral load of the columns also started to decrease with an increase of the lateral displacement after reaching their peak load. Many researchers have explained the reasons for the degradation (e.g., Ang 1985; Cai et al. 2015) and indicated that the degradation of RC columns with increasing lateral displacement is very important in terms of safety aspects of structures subjected to strong earthquakes. To promote the performance- or drift-based design of RC structures subjected to strong earthquakes, Cai et al. (2015) proposed a complete shear design model for circular concrete columns which was able to predict the degradation of the lateral shear resistance of the columns under a megaearthquake. Cai et al. (2015) pointed out that the effective lateral confinement factor (I_c) of circular RC columns had a significant influence on the peak drift ratio of the columns, which they called the degradation-starting drift ratio R_{iu}. The drift ratio is calculated as the ratio Δ_{max}/L, where Δ_{max} is the displacement corresponding to the peak load point, and L is the shear span of

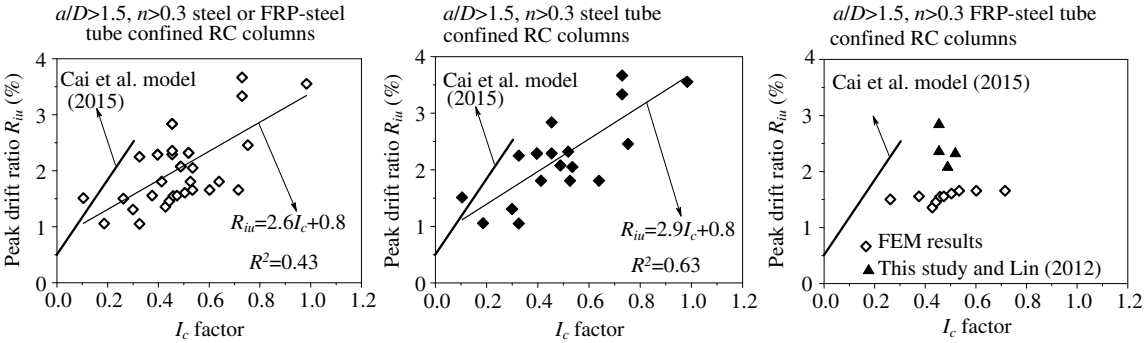

Fig. 23. Relationship of peak drift ratio and I_c factor of confined RC columns.

the columns. To discuss the drift ratio of the confined RC columns, this study collected several RC columns confined by steel tube or FRP–steel tube from the existing literature (Liu et al. 2009; Zhou and Liu 2010; Gan et al. 2011; Lin 2012). Using the FEM analysis results in this paper, a data set of the confined RC columns with shear span ratios (a/D) larger than 1.5 and axial load ratios (n) exceeding of 0.3 was modeled and analyzed. In theory, these columns have a stronger trend to fail in flexural failure mode. In the model developed by Cai et al. (2015), the effective lateral confinement factor (I_c) of FRP–steel-confined RC columns is calculated by

$$I_c = \frac{\rho_{hs} \cdot f_{hs}}{f_{co}} + \frac{\rho_{hst} \cdot f_{hst}}{f_{co}} + \frac{\rho_{hfrp} \cdot f_{hfrp}}{f_{co}} \tag{10}$$

where ρ_{hs} = volume ratio of stirrup; ρ_{hst} and ρ_{hfrp} = equivalent stirrup volume ratio of the steel tube and the FRP tube, respectively; f_{hs} and f_{hst} = yield strength of the stirrup and the steel tube, respectively; and f_{hfrp} = hoop stress of the FRP tube at the peak point, taken as about 10% of the ultimate strength of FRP according to the test results.

Fig. 23 shows the relationship between peak drift ratio R_{iu} and the effective lateral confinement factor I_c of the columns confined by the steel or FRP–steel tubes. The factor I_c had a different influence on the peak drift level of circular confined RC columns compared with the case of circular RC columns. According to existing design codes, most circular RC columns have an I_c factor less than 0.3 and have a peak drift varying from 0.5% to 2.5%. The increase of I_c caused a larger increase in the peak drift ratio in Cai et al.'s (2015) model. This can be explained by the fact that the increase of lateral confinement of RC columns has a more significant effect on the enhancement of peak drift ratio of shear-dominant columns. In the data established in the paper, however, all confined columns were flexural-dominant columns. Furthermore, the I_c factors of the RC columns confined by steel or FRP–steel tubes had a larger varying region. The peak drifts ratios of the columns increased with the I_c factors. Compared with the case of steel tube–confined or FRP–steel tube–confined RC columns, a stronger linear relationship was found between the I_c factor and the peak drift ratio R_{iu} of steel tube–confined RC columns. However, the existing data of FRP–steel tube–confined columns was not sufficient to determine the relationship between I_c and R_{iu} in these columns (Fig. 23). Therefore, the paper suggests that peak drift ratio R_{iu} of the RC columns confined by steel tubes or FRP–steel tubes can be calculated simply by

$$R_{iu} = 2.6I_c + 0.8(\%) \tag{11}$$

Concluding Remarks

This paper investigated the behavior of FRP–steel-confined concrete columns under reversed cyclic lateral loads through a series of experiments, including RC (reference column), steel tube–confined RC/SRC columns, and FRP–steel-confined RC/SRC columns. Flexural failures were observed for all columns. The following conclusions can be made:

- With the increase of the number of FRP layers, the structural behaviors (including yield load and displacement, peak load and displacement, ultimate load and displacement, and ductility coefficient) of the FRP–steel-confined RC/SRC columns improved.
- The load-carrying capacity, ductility, and energy dissipation capacity of FRP–steel-confined RC columns were better than those of RC columns and steel tube–confined RC columns. Moreover, the improvement caused by the lateral confinement increased as the number of layers of FRP increased. Similar results occurred in FRP–steel-confined SRC columns compared with SRC columns or steel tube–confined SRC columns.
- FRP wrapping had no significant effect on the initial stiffness of FRP–steel-confined RC/SRC columns. However, with the increase of the lateral displacement and with more layers of FRP sheet confining, the stiffness degradation of the columns decreased.

Based on the proposed FEM model verified by the test results in the paper, a parametric analysis was conducted to analyze main factors influencing the behavior of GFRP–steel-confined RC columns. The main observations are as follows:

- With the increase of the axial load ratio and the shear span ratio, the load-bearing capacity of steel tube–confined and FRP–steel-confined RC columns improved, whereas the ductility of the columns significantly decreased.
- The load-bearing capacity of steel tube–confined and FRP–steel-confined RC columns increased as the thickness of steel tube increased; that of the former kind of columns increased more significantly. However, the thickness had no significant influence on the ductility of the columns.
- The increase of the longitudinal reinforcement ratio improved the load-bearing capacity of steel tube–confined and FRP–steel-confined RC columns but had little effect on the ductility of the columns.
- The increase of the number of FRP layers enhanced the ultimate load-bearing capacity and ductility of FRP–steel-confined RC columns, but the effect decreased after a certain number of FRP layers was applied. More studies are needed to quantify this for FRP–steel-confined RC columns. The change in the height of FRP wrapping had no significant influence on the

load-bearing capacity and ductility the columns after the height reached 1.5 times the column diameter.

This study also discussed the influence of main variables on the plastic hinge region height and peak drift ratio of the confined RC columns under reversed cyclic loads and showed that the lateral confinement condition has a significant influence on the PHR height and peak drift ratio of the confined RC columns. Based on the existing test data, the paper suggests a simple model to predict the peak drift ratio of the confined RC columns.

Acknowledgments

This work was supported by the National Key R&D Program of China (Project No. 2017YFC0703007), the National Natural Science Foundation of China (Project Nos. 51778102 and 51708433), the Fundamental Research Funds for the Central Universities (Project No. DUT18LK35), and the Natural Science Foundation of Liaoning Province of China (Project No. 20180550763).

References

Aboutaha, R. S., and R. I. Machado. 1999. "Seismic resistance of steel-tubed high-strength reinforced-concrete columns." *J. Struct. Eng.* 125 (5): 485–494. https://doi.org/10.1061/(ASCE)0733-9445(1999)125:5(485).

Ang, B. G. 1985. *Seismic shear strength of circular bridge piers*. Rep. No. 85-5. Christchurch, New Zealand: Univ. of Canterbury.

Bae, S., and O. Bayrak. 2008. "Plastic hinge length of reinforced concrete columns." *ACI Struct. J.* 105 (3): 290–300.

Binici, B. 2005. "An analytical model for stress-strain behavior of confined concrete." *Eng. Struct.* 27 (7): 1040–1051. https://doi.org/10.1016/j.engstruct.2005.03.002.

Cai, G., Y. Sun, T. Takeuchi, and J. Zhang. 2015. "Proposal of a complete seismic shear strength model for circular concrete columns." *Eng. Struct.* 100: 399–409. https://doi.org/10.1016/j.engstruct.2015.06.032.

Cao, Q., J. Tao, Z. Wu, and Z. J. Ma. 2017. "Behavior of FRP-steel confined concrete tubular columns made of expansive self-consolidating concrete under axial compression." *J. Compos. Constr.* 21 (5): 04017037. https://doi.org/10.1061/(ASCE)CC.1943-5614.0000818.

Chinese Standards. 2002. *Technical specification for concrete structures of tall buildings*. [In Chinese.] JGJ3-2002. Beijing: Standardization Administration of the People's Republic of China.

Chinese Standards. 2009. *Tensile test method for the metal materials at room temperature*. [In Chinese.] GB/T228-2010. Beijing: Standardization Administration of the People's Republic of China.

Chinese Standards. 2015. *Code for design of concrete structures*. [In Chinese.] GB 50010-2010. Beijing: Ministry of House and Urban-Rural Development of People's Republic of China.

Gan, D., L. Guo, J. Liu, and X. Zhou. 2011. "Seismic behavior and moment strength of tubed steel reinforced-concrete (SRC) beam-columns." *J. Constr. Steel Res.* 67 (10): 1516–1524. https://doi.org/10.1016/j.jcsr.2011.03.025.

Han, L. H., W. Liu, and Y. F. Yang. 2008. "Behavior of thin walled steel tube confined concrete stub columns subjected to axial local compression." *Thin Wall Struct.* 46 (2): 155–164. https://doi.org/10.1016/j.tws.2007.08.029.

Han, L. H., H. Qu, Z. Tao, and Z. F. Wang. 2009. "Experimental behaviour of thin-walled steel tube confined concrete column to RC beam joints under cyclic loading." *Thin Wall Struct.* 47 (8–9): 847–857. https://doi.org/10.1016/j.tws.2009.03.001.

Han, L. H., G. H. Yao, Z. B. Chen, and Q. Yu. 2005. "Experimental behaviours of steel tube confined concrete (STCC) columns." *Steel Compos. Struct.* 5 (6): 459–484. https://doi.org/10.12989/scs.2005.5.6.459.

Hu, H., and R. Seracino. 2014. "Analytical model for FRP-and-steel-confined circular concrete columns in compression." *J. Compos. Constr.* 18 (3): A4013012. https://doi.org/10.1061/(ASCE)CC.1943-5614.0000394.

Hu, Y. M. 2011. "Behaviour and modelling of FRP-confined hollow and concrete-filled steel tubular columns." Ph.D. dissertation, Dept. of Civil and Environmental Engineering, Hong Kong Polytechnic Univ.

Hu, Y. M., T. Yu, and J. G. Teng. 2011. "FRP-confined circular concrete-filled thin steel tubes under axial compression." *J. Compos. Constr.* 15 (5): 850–860. https://doi.org/10.1061/(ASCE)CC.1943-5614.0000217.

Huang, P. D. 2016. "Cyclic axial compression mechanical behavior study of GFRP-steel composite tube confined RC stub columns." [In Chinese.] M.S. thesis, Dept. of Civil Engineering, Dalian Univ. of Technology.

Inel, M., and H. B. Ozmen. 2006. "Effects of plastic hinge properties in nonlinear analysis of reinforced concrete buildings." *Eng. Struct.* 28 (11): 1494–1502. https://doi.org/10.1016/j.engstruct.2006.01.017.

Jiang, T., and J. G. Teng. 2007. "Analysis-oriented models for FRP-confined concrete." *Eng. Struct.* 29 (11): 2968–2986. https://doi.org/10.1016/j.engstruct.2007.01.010.

Kent, D. C., and R. Park. 1971. "Flexural members with confined concrete." *J. Struct. Div.* 97 (7): 1969–1990.

Lam, L., and J. G. Teng. 2009. "Stress-strain model for FRP-confined concrete under cyclic axial compression." *Eng. Struct.* 31 (2): 308–321. https://doi.org/10.1016/j.engstruct.2008.08.014.

Li, Y. F., S. H. Chen, K. C. Chang, and K. Y. Liu. 2005. "A constitutive model of concrete confined by steel reinforcements and steel jackets." *Can. J. Civ. Eng.* 32 (1): 279–288. https://doi.org/10.1139/l04-093.

Lin, S. L. 2012. "Seismic performance of FRP-steel composite tube confined RC columns." [In Chinese.] M.S. thesis, Dept. of Civil Engineering, Harbin Institute of Technology.

Liu, J., and S. A. Sheikh. 2013. "Fiber-reinforced polymer-confined circular columns under simulated seismic loads." *ACI Struct. J.* 110 (6): 941.

Liu, J., S. Zhang, X. Zhang, and L. Guo. 2009. "Behavior and strength of circular tube confined reinforced-concrete (CTRC) columns." *J. Constr. Steel Res.* 65 (7): 1447–1458. https://doi.org/10.1016/j.jcsr.2009.03.014.

Liu, J. P., T. X. Xu, Y. H. Wang, and Y. Guo. 2018. "Axial behaviour of circular steel tubed concrete stub columns confined by CFRP materials." *Constr. Build Mater.* 168: 221–231. https://doi.org/10.1016/j.conbuildmat.2018.02.131.

Liu, L., and Y. Lu. 2010. "Axial bearing capacity of short FRP confined concrete-filled steel tubular columns." *J. Wuhan Univ. Tech.-Mater. Sci. Ed.* 25 (3): 454–458. https://doi.org/10.1007/s11595-010-0022-2.

Mazzoni, S., F. McKenna, M. H. Scott, and G. L. Fenves. 2006. *OpenSees command language manual*. Berkeley, CA: Pacific Earthquake Engineering Research Center.

Menegotto, M., and E. Pinto. 1973. "Method of analysis for cyclically loaded reinforced concrete plane frames including changes in geometry and non-elastic behavior of elements under combined normal force and bending." In *Proc., IABSE Symp.*, 15–22. Zurich, Switzerland: IABSE.

Orakcal, K., L. M. Massone, and J. W. Wallence. 2006. *Analytical modeling of reinforced concrete walls for predicting flexural and coupled-shear-flexural responses*. Berkeley, CA: Univ. of California, Berkeley.

Ozbakkaloglu, T., and Y. Idris. 2014. "Seismic behavior of FRP-high-strength concrete-steel double-skin tubular columns." *J. Struct. Eng.* 140 (6): 04014019. https://doi.org/10.1061/(ASCE)ST.1943-541X.0000981.

Ozbakkaloglu, T., and M. Saatcioglu. 2006. "Seismic behavior of high-strength concrete columns confined by fiber-reinforced polymer tubes." *J. Compos. Constr.* 10 (6): 538–549. https://doi.org/10.1061/(ASCE)1090-0268(2006)10:6(538).

Ozbakkaloglu, T., and M. Saatcioglu. 2007. "Seismic performance of square high-strength concrete columns in FRP stay-in-place formwork." *J. Struct. Eng.* 133 (1): 44–56. https://doi.org/10.1061/(ASCE)0733-9445(2007)133:1(44).

Park, J. W., and S. M. Choi. 2013. "Structural behavior of CFRP strengthened concrete-filled steel tubes columns under axial compression loads." *Steel Compos. Struct.* 14 (5): 453–472. https://doi.org/10.12989/scs.2013.14.5.453.

Park, J. W., Y. K. Hong, and S. M. Choi. 2010. "Behaviors of concrete filled square steel tubes confined by carbon fiber sheets (CFS) under

compression and cyclic loads." *Steel Compos. Struct.* 10 (2): 187–205. https://doi.org/10.12989/scs.2010.10.2.187.

Park, R. 1988. "State of the art report ductility evaluation from laboratory and analytical testing." In *Proc., 9th World Conf. on Earthquake Engineering*, 605–616. Tokyo: International Association for Earthquake Engineering.

Popovics, S. 1973. "A numerical approach to the complete stress-strain curve of concrete." *Cem. Concr. Res.* 3 (5): 583–599. https://doi.org/10.1016/0008-8846(73)90096-3.

Ran, J. H. 2014. "Axial compression mechanical behavior of FRP-steel composite tube confined concrete stub columns." [In Chinese.] M.S. thesis, Dept. of Civil Engineering, Dalian Univ. of Technology.

Sakino, K., H. Nakahara, S. Morino, and I. Nishiyama. 2004. "Behavior of centrally loaded concrete-filled steel-tube short columns." *J. Struct. Eng.* 130 (2): 180–188. https://doi.org/10.1061/(ASCE)0733-9445(2004)130:2(180).

Scott, B. D., R. Park, and M. J. N. Priestley. 1982. "Stress-strain behavior of concrete confined by overlapping hoops at low and high strain rates." *ACI Struct. J.* 79 (1): 13–27.

Tao, Z., Z. Wang, L. Han, and B. Uy. 2011. "Fire performance of concrete-filled steel tubular columns strengthened by CFRP." *Steel Compos. Struct.* 11 (4): 307–324. https://doi.org/10.12989/scs.2011.11.4.307.

Teng, J. G., J. F. Chen, S. T. Smith, and L. Lam. 2002. *FRP: Strengthened RC structures*. Weinheim, Germany: Wiley.

Teng, J. G., Y. M. Hu, and T. Yu. 2013. "Stress-strain model for concrete in FRP-confined steel tubular columns." *Eng. Struct.* 49 (2): 156–167. https://doi.org/10.1016/j.engstruct.2012.11.001.

Tomii, M., K. Sakino, K. Watanabe, and Y. Xiao. 1985a. "Lateral load capacity of reinforced concrete short columns confined by steel tube." In *Proc., Int. Specialty Conf. on Concrete-Filled Steel Tubular Structures*, 19–26. Harbin, China: Harbin Institute of Technology.

Tomii, M., K. Sakino, Y. Xiao, and K. Watanabe. 1985b. "Earthquake resisting hysteretic behavior of reinforced concrete short columns confined by steel tube." In *Proc., Int. Speciality Conf. on Concrete Filled Steel Tubular Structures*, 119–125. Harbin, China: Harbin Institute of Technology.

Wang, Z., Q. Yu, and Z. Tao. 2015. "Behaviour of CFRP externally-reinforced circular CFT members under combined tension and bending." *J. Constr. Steel Res.* 106: 122–137. https://doi.org/10.1016/j.jcsr.2014.12.007.

Wu, Z., X. Wang, X. Zhao, and M. Noori. 2014. "State-of-the-art review of FRP composites for major construction with high performance and longevity." *J. Sustainable Mater. Struct. Syst.* 1 (3): 201–231. https://doi.org/10.1504/IJSMSS.2014.062757.

Xiao, Y. 2004. "Applications of FRP composites in concrete columns." *Adv. Struct. Eng.* 7 (4): 335–343. https://doi.org/10.1260/1369433041653552.

Xiao, Y., W. He, and K. K. Choi. 2005. "Confined concrete-filled tubular columns." *J. Struct. Eng.* 131 (3): 488–497. https://doi.org/10.1061/(ASCE)0733-9445(2005)131:3(488).

Youssf, O., M. A. ElGawady, and J. E. Mills. 2015. "Displacement and plastic hinge length of FRP-confined circular reinforced concrete columns." *Eng. Struct.* 101: 465–476. https://doi.org/10.1016/j.engstruct.2015.07.026.

Yu, Q., Z. Tao, W. Liu, and Z. B. Chen. 2010. "Analysis and calculations of steel tube confined concrete (STCC) stub columns." *J. Constr. Steel Res.* 66 (1): 53–64. https://doi.org/10.1016/j.jcsr.2009.08.003.

Yu, T., Y. M. Hu, and J. G. Teng. 2016. "Cyclic lateral response of FRP-confined circular concrete-filled steel tubular columns." *J. Constr. Steel Res.* 124: 12–22. https://doi.org/10.1016/j.jcsr.2016.05.006.

Yuan, F., Y. F. Wu, and C. Q. Li. 2017. "Modelling plastic hinge of FRP-confined RC columns." *Eng. Struct.* 131: 651–668. https://doi.org/10.1016/j.engstruct.2016.10.018.

Zhou, X., G. Cheng, J. Liu, D. Gan, and Y. F. Chen. 2017. "Behavior of circular tubed-RC column to RC beam connections under axial compression." *J. Constr. Steel Res.* 130: 96–108. https://doi.org/10.1016/j.jcsr.2016.12.005.

Zhou, X. H., and J. P. Liu. 2010. "Seismic behavior and shear strength of tubed RC short columns." *J. Constr. Steel Res.* 66 (3): 385–397. https://doi.org/10.1016/j.jcsr.2009.10.011.

Zhou, X. H., J. P. Liu, X. Wang, and Y. F. Chen. 2016. "Behavior and design of slender circular tubed-reinforced-concrete columns subjected to eccentric compression." *Eng. Struct.* 124: 17–28. https://doi.org/10.1016/j.engstruct.2016.05.036.

Zhou, X. H., B. Yan, and J. P. Liu. 2015. "Behavior of square tubed steel reinforced-concrete (SRC) columns under eccentric compression." *Thin Wall Struct.* 91: 129–138. https://doi.org/10.1016/j.tws.2015.01.022.